Thin-Walled Structures 189 (2023) 110849

Contents lists available at ScienceDirect

Thin-Walled Structures

journal homepage: www.elsevier.com/locate/tws

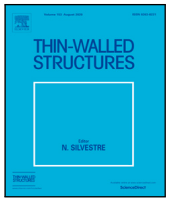

Full length article

Simulation and cross-section resistance of stainless steel SHS and RHS at elevated temperatures

Chunyan Quan, Merih Kucukler *

School of Engineering, University of Warwick, Coventry, CV4 7AL, UK

ARTICLE INFO

Keywords:
Cross-section resistance
Elevated temperature
Finite element modelling
Fire
Rectangular hollow sections (RHS)
Square hollow sections (SHS)
Stainless steel

ABSTRACT

This paper investigates the structural response and design of stainless steel square and rectangular hollow sections (SHS and RHS) at elevated temperatures. Finite element models able to replicate the behaviour of stainless steel SHS and RHS members at elevated temperatures are developed and verified against the results from physical experiments, which are then used to perform extensive numerical parametric studies to generate a broad range of benchmark structural performance data on the behaviour of stainless steel SHS and RHS at elevated temperatures. In total, 13860 cold-formed and hot-rolled austenitic, duplex and ferritic stainless steel SHS and RHS with a wide range of cross-section properties and subjected to various loading conditions at different elevated temperature levels are considered. A cross-section design method for stainless steel SHS and RHS under different loading conditions at elevated temperatures is proposed, considering the recent design recommendations in [1] for the local buckling assessment of stainless steel plates at elevated temperatures which will be included in the upcoming version of the European structural steel fire design standard EN 1993-1-2. Relative to the current local buckling assessment rules of EN 1993-1-2, the higher accuracy, safety and reliability of the new proposals in the estimations of the ultimate cross-section resistances of stainless steel SHS and RHS at elevated temperatures are demonstrated.

1. Introduction

The use of stainless steel in the construction and offshore industries has been growing in view of its excellent corrosion resistance, high durability, low maintenance costs and aesthetic appearance [1]. Owing to the variations in its chemical composition relative to carbon steel, stainless steel displays considerably different elevated temperature material response, exhibiting superior strength and stiffness retention at elevated temperatures relative to carbon steel [2]. However, currently, the superior fire performance of stainless steel is not sufficiently exploited in the fire design of stainless steel structures due to the lack of specific fire design rules in structural steel fire design standards such the European structural steel fire design standard EN 1993-1-2 [3], highlighting that the establishment of bespoke fire design rules for stainless steel structures furnishing accurate estimations of their behaviour at elevated temperatures is necessary [4].

In both room temperature and elevated temperature design of stainless steel cross-sections, the adverse influence of local instability effects on the ultimate cross-section resistances must be taken into consideration. To account for the detrimental influence of local buckling at elevated temperatures, the current European structural steel fire design standard EN 1993-1-2 [3] recommends the use of the room temperature local buckling assessment equations provided in the European room temperature stainless steel design standard EN 1993-1-4 [5]. However, these room temperature design equations provided in EN 1993-1-4 [5] were originally developed taking into account the room temperature local buckling response of stainless steel plates and cross-sections, thus failing to accurately account for the local buckling behaviour at elevated temperatures. To address the inaccuracy of EN 1993-1-2 [3] in the local buckling assessment of steel cross-sections at elevated temperatures, a number of relevant research studies have been performed recently. In Ranby [6], the use of room temperature local buckling assessment methods with the elevated temperature steel material strengths is recommended for the determination of the local buckling resistances of steel cross-sections at elevated temperatures. According to the recommendations of Ranby [6], in view of the attainment of high strain levels in Class 1, 2 and 3 (non-slender) steel cross-sections at elevated temperatures, the elevated temperature material strengths at 2% total strain $f_{2,\theta}$ can be used as the reference material strengths for their fire design. On the other hand, Ranby [6] recommended that considering the low probability of the attainment of high strain levels in Class 4 (slender) cross-sections, the elevated temperature 0.2% proof strengths $f_{p0.2,\theta}$ can be used as the reference material strengths for their fire design. The described recommendations

* Corresponding author.
E-mail address: merih.kucukler@warwick.ac.uk (M. Kucukler).

https://doi.org/10.1016/j.tws.2023.110849
Received 21 January 2023; Received in revised form 6 April 2023; Accepted 9 May 2023
Available online 13 June 2023

of Ranby [6] have been adopted in the current version of EN 1993-1-2 [3] for the local buckling assessment of both carbon steel and stainless steel cross-sections at elevated temperatures. However, recently, the limitations of EN 1993-1-2 [3] in the local buckling assessment of steel sections at elevated temperatures have been highlighted [7,8]: (i) EN 1993-1-2 [3] may lead to inaccurate ultimate resistance predictions for steel cross-sections at elevated temperatures and (ii) the adoption of the elevated temperature material strengths $f_{2,\theta}$ for the fire design of Class 1, 2 and 3 sections and $f_{p0.2,\theta}$ for the fire design of Class 4 sections results in artificial steps in the resistance predictions at the transitions from Class 3 to Class 4 cross-sections. To eliminate these shortcomings, Couto et al. [8] recommended the consistent use of $f_{2,\theta}$ as the reference material strengths with a new effective width method for the resistance predictions for all classes of carbon steel cross-sections at elevated temperatures. Xing et al. [9] investigated the local buckling behaviour of stainless steel plates at elevated temperatures and proposed a new effective width method for predicting their ultimate resistances. In line with [8], Xing et al. [9] recommended the use of $f_{2,\theta}$ as the reference material strengths for the determination of the ultimate resistances of stainless steel cross-sections at elevated temperatures regardless of their cross-section class. The new fire design rules and effective width method for stainless steel cross-sections proposed in Xing et al. [9] will be incorporated into the upcoming version of the European structural steel fire design standard which is currently referred to as prEN 1993-1-2 [10]. In Xing et al. [11], the design recommendations of [9] were extended to the fire design of welded stainless steel I-sections, where it was shown that the design recommendations of [9] lead to more accurate and reliable ultimate resistance predictions for stainless steel I-sections at elevated temperatures relative to the local buckling assessment rules of EN 1993-1-2 [3]. However, in Xing et al. [11], only stainless steel welded I-sections subjected to pure axial compression or pure bending at elevated temperatures were taken into consideration; the behaviour and design of stainless steel square hollow sections (SHS) and rectangular hollow sections (RHS) at elevated temperatures were not investigated. Additionally, [12,13] investigated the structural response of cold-formed stainless steel SHS and RHS columns and beam–columns at elevated temperatures and assessed the accuracy of the existing fire design methods. However, these studies primarily focused on the global buckling behaviour.

To this end, a comprehensive research study on the structural response and design of stainless steel SHS and RHS at elevated temperatures is carried out in this study. A large number of cold-formed and hot-rolled stainless steel SHS and RHS subjected to (i) pure axial compression, (ii) pure bending, (iii) combined axial compression and bending and (iv) combined bending and shear at elevated temperatures are considered. Note that although hot-rolled structural stainless steel SHS and RHS are significantly less common relative to cold-formed stainless steel SHS and RHS, such sections have been introduced to the industry [14]. Therefore, in this study, in addition to cold-formed stainless steel SHS and RHS, hot-rolled stainless steel SHS and RHS are also investigated. Following the development of the effective width method for individual stainless steel plates at elevated temperatures in [9], in this study, a cross-section design method for stainless steel SHS and RHS is established, considering the effective width method put forward in [9]. The basis and main principles of the effective width method put forward in [9] and its accuracy for individual stainless steel plates at elevated temperatures are first described. Then, the accuracy and reliability of the new design proposals proposed in this study for stainless steel SHS and RHS subjected to different loading conditions are thoroughly verified against the benchmark structural performance data obtained from shell finite element (FE) modelling, considering austenitic, duplex and ferritic stainless steel grades, various cross-section slendernesses and elevated temperatures. Note that the behaviour and design of cold-formed and hot-rolled stainless steel circular hollow sections (CHS) and elliptical hollow sections (EHS) at elevated temperatures have also been investigated in a parallel research study [15], where new cross-section design equations leading to accurate ultimate resistance predictions for stainless steel CHS and EHS at elevated temperatures have been put forward.

2. Finite element modelling

In this study, shell finite element models were developed to replicate the structural response of stainless steel SHS and RHS at elevated temperatures. Geometrically and Materially Nonlinear Analyses with Imperfections (GMNIA) of the shell finite element models were performed, thereby generating extensive benchmark structural performance data against which (i) the design approach proposed in this study and (ii) the design rules existing in EN 1993-1-2 [3] were assessed for the ultimate resistance predictions of stainless steel SHS and RHS at elevated temperatures. This section sets out the development and verification of the shell finite element models and the scope of the extensive parametric studies performed by means of the verified shell finite element models.

2.1. Development of finite element models

2.1.1. Modelling approach

The finite element analysis software Abaqus [16] was used in the finite element modelling of the structural response of stainless steel SHS and RHS members at elevated temperatures in this study. The four-noded shell finite element with reduced integration referred to as S4R in the Abaqus [16] element library, which has been successfully used in previous studies for similar applications [17,18], was employed to create all the finite element models. Employing suitable boundary conditions, a symmetry plane was exploited at the midspan and an additional symmetry plane was also exploited through the member length for the SHS and RHS members, thereby producing computationally efficient quarter models for the SHS and RHS members as shown in Fig. 1. The accuracy of the generated quarter SHS and RHS models was verified against the results obtained from the corresponding full models. In the finite element models, all the six degrees of freedom at the end sections were linked to the reference nodes through kinematic coupling, which ensured the translational and rotational degrees of freedom of all nodes at the end sections being identical to those of the corresponding reference nodes and also prevented localised failure; this same approach has also been adopted in the FE models of [19] where the cross-section behaviour of steel hollow sections was investigated. The loading and boundary conditions were applied to the reference nodes to which the nodes with the end sections were coupled. For the stub columns, fixed end support boundary conditions were employed by restraining all the degrees of freedom with the exception of the longitudinal displacement at the loaded end (i.e. $u_y = u_z = r_x = r_y = r_z = 0$). For the stub beam–columns and beams, pin-ended boundary conditions about the bending axis were established at the reference nodes by releasing the rotation about the bending axis (i.e. $u_y = u_z = r_x = r_z = 0$, but $r_y \neq 0$). For the 3-point bending cases, all the degrees of freedom at the midspan section were linked to a reference node through rigid body and a vertical load V_{Ed} was applied to this reference node. On the other hand, for the other loading cases (i.e. pure axial compression, pure bending and combined axial compression and bending), concentric and eccentric axial forces N_{Ed} and bending moments M_{Ed} were applied to the reference nodes at the ends, as shown in Fig. 1.

Relative to hot-rolled stainless steel SHS and RHS, cold-formed stainless steel SHS and RHS typically have larger corner radii to avoid corner crackling during their manufacture in the cold-rolling procedure [20]. In this study, the external corner radii r specified in EN 10219-2 [21] and EN 10210-2 [22] were adopted. Thus, the external corner radii r were taken as two times of the cross-section thicknesses t (i.e. $r = 2t$) for cold-formed SHS and RHS, while the corner radii r were taken as 1.5 times of the cross-section thicknesses t (i.e. $r = 1.5t$) for hot-rolled SHS and RHS. To accurately capture the elastic–plastic cross-section response within the finite element models, a fine mesh with shell element size equal to the cross-section thickness t was adopted in the flat regions of SHS and RHS in line with the adoption in [23] based on a mesh sensitivity study; while in the corner regions, four

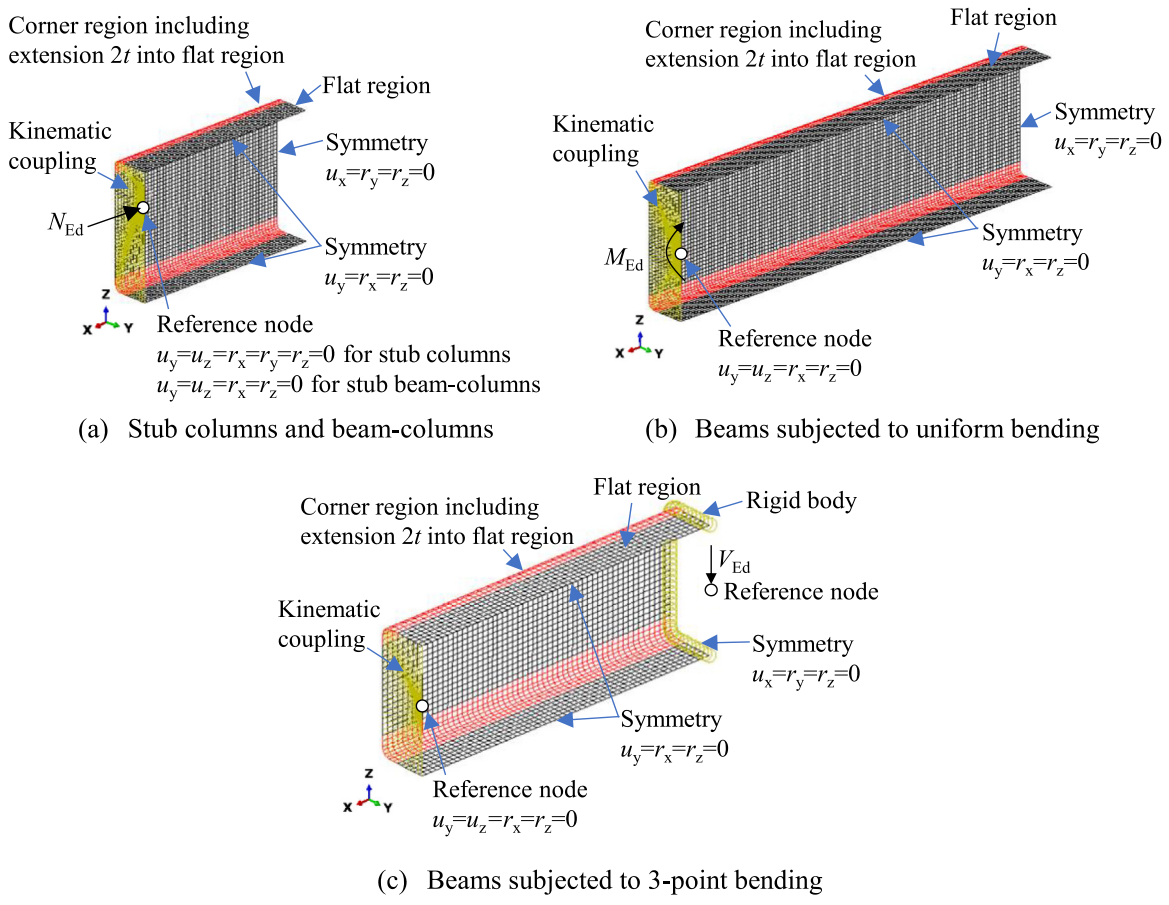

Fig. 1. Details of the finite element models of SHS/RHS developed in this study.

elements were employed to accurately capture the curved geometry in line with [24]. The element size along the member length was selected such that the aspect ratios of the elements were approximately equal to unity. The Simpson integration method was adopted and five integration points were employed through the thicknesses of the shell elements [16]. The isothermal analysis technique was used in the finite element simulations, where the temperatures of the finite element models were initially increased to predefined elevated temperature levels θ which led to the development of thermal strains and the modification of the material behaviour, and then the loading was applied to the finite element models at the predefined elevated temperature levels θ up to failure. The maximum values of the applied loads were assumed as the ultimate load carrying capacities of the finite element models at the predefined elevated temperature levels θ. The modified Riks analysis [16] was employed to determine the full load–deformation response of the finite element models in the all numerical simulations, including the post-ultimate response.

2.1.2. Material modelling

The structural fire response of both cold-formed and hot-rolled stainless steel SHS and RHS was taken into consideration in this paper. For each stainless steel family, one typical grade was selected: 1.4301 austenitic (A), 1.4462 duplex (D) and 1.4003 ferritic (F). In this study, the two-stage Ramberg–Osgood material model [25–27] was used to express the full stress–strain $\sigma-\varepsilon$ response at temperature θ, as given by Eqs. (1)–(2) and illustrated in Fig. 2, where E_θ is the Young's modulus at temperature θ, $E_{p0.2\theta}$ is the tangent modulus at the 0.2% proof stress $f_{p0.2,\theta}$ as given by Eq. (3), $\varepsilon_{p0.2,\theta}$ is the total strain at $f_{p0.2,\theta}$ equal to $0.002+f_{p0.2,\theta}/E_\theta$, $f_{u,\theta}$ and $\varepsilon_{u,\theta}$ are the ultimate strength and strain at temperature θ, and n_θ and m_θ are the strain hardening exponents, respectively.

$$\varepsilon = \frac{\sigma}{E_\theta} + 0.002\left(\frac{\sigma}{f_{p0.2,\theta}}\right)^{n_\theta} \quad \text{for } \sigma \le f_{p0.2,\theta} \tag{1}$$

$$\varepsilon = \varepsilon_{p0.2,\theta} + \frac{\sigma - f_{p0.2,\theta}}{E_{p0.2,\theta}} + \left(\varepsilon_{u,\theta} - \varepsilon_{p0.2,\theta} - \frac{f_{u,\theta} - f_{p0.2,\theta}}{E_{p0.2,\theta}}\right)\left(\frac{\sigma - f_{p0.2,\theta}}{f_{u,\theta} - f_{p0.2,\theta}}\right)^{m_\theta}$$
$$\text{for } f_{p0.2,\theta} < \sigma \le f_{u,\theta} \tag{2}$$

$$E_{p0.2,\theta} = \frac{E_\theta}{1 + 0.002 n_\theta \frac{E_\theta}{f_{p0.2,\theta}}} \tag{3}$$

The material properties at elevated temperatures (i.e. $f_{p0.2,\theta}$, $f_{2,\theta}$, $f_{u,\theta}$, $\varepsilon_{u,\theta}$, E_θ) utilised in Eqs. (1)–(3) were determined by multiplying the material properties at room temperature, i.e. the yield (0.2% proof) stress f_y, ultimate stress f_u, ultimate strain ε_u and Young's modulus E, by the corresponding strength ($k_{p0.2,\theta}$, $k_{2,\theta}$, $k_{u,\theta}$), ductility ($k_{\varepsilon u,\theta}$) and stiffness ($k_{E,\theta}$) reduction factors provided in the Steel Construction Institute (SCI) Design Manual for Structural Stainless Steel [30], which are based on the results from the extensive elevated temperature material tests carried out in [28,31–33], thus $f_{p0.2,\theta} = k_{p0.2,\theta} f_y$, $f_{2,\theta} = k_{2,\theta} f_y$, $f_{u,\theta} = k_{u,\theta} f_u$, $\varepsilon_{u,\theta} = k_{\varepsilon u,\theta}\varepsilon_u$ and $E_\theta = k_{E,\theta}E$. Note that the material reduction factors for stainless steel provided in [30] will be incorporated into the upcoming version of the European structural steel fire design standard EN 1993-1-2 [3] in conjunction with the two stage Ramberg–Osgood material model given by Eqs. (1)–(2). Thus, the elevated temperature material modelling approach employed in this study is in accordance with the provisions provided in the upcoming version of the European structural steel fire design standard EN 1993-1-2 [3] for the elevated temperature material modelling of stainless steel. The standardised room temperature material properties recommended in [34] for (i) cold-formed stainless steel SHS and RHS (flat and corner

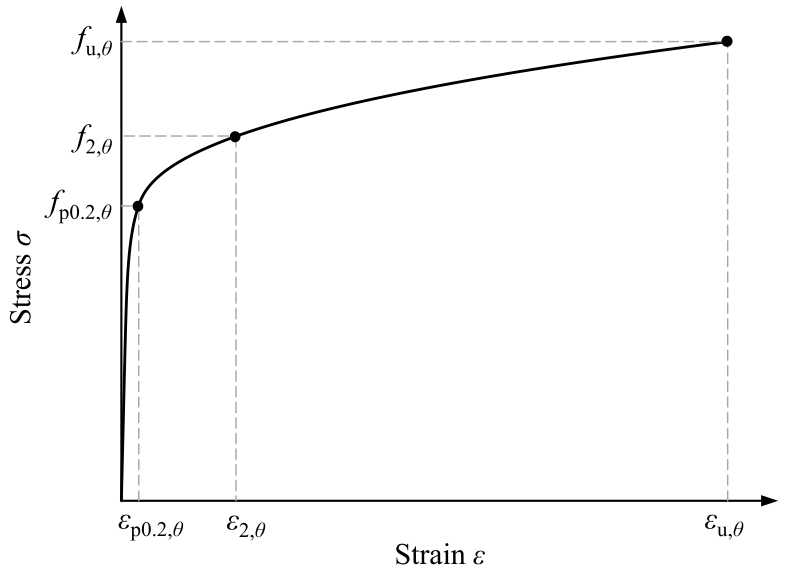

Fig. 2. Two-stage elevated temperature Ramberg–Osgood material model for stainless steel [25–27].

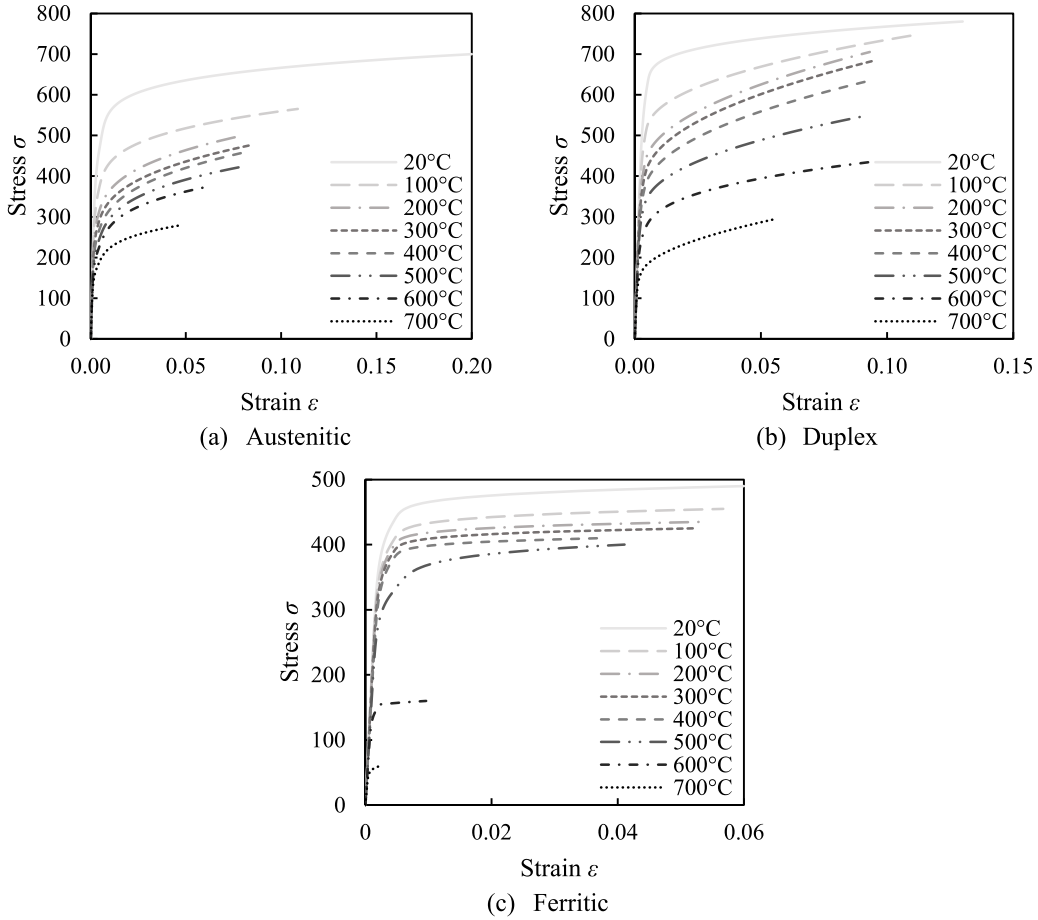

Fig. 3. Stress–strain curves of flat portions of cold-formed stainless steel at elevated temperatures.

regions) and (ii) hot-rolled stainless steel SHS and RHS were employed in this study in line with [12], as provided in Table 1. For the hot-rolled stainless steel SHS and RHS, the material properties were uniformly applied to the cross-sections. In the case of the cold-formed stainless steel SHS and RHS, the strength enhancements arising in the corner regions due to the plastic deformations during the rolling process were considered. Thus, the enhanced material properties for the corner regions of cold-formed stainless steel SHS and RHS recommended in [34] and shown in Table 1 were used in the corner regions of the modelled cold-formed stainless steel SHS and RHS, with extensions into the flat regions taken equal to two times of the cross-section thicknesses $2t$ [35], as shown in Fig. 1. The elevated temperature material properties obtained in [36,37] indicate that the material strength enhancements induced due to the cold-work at room temperature can

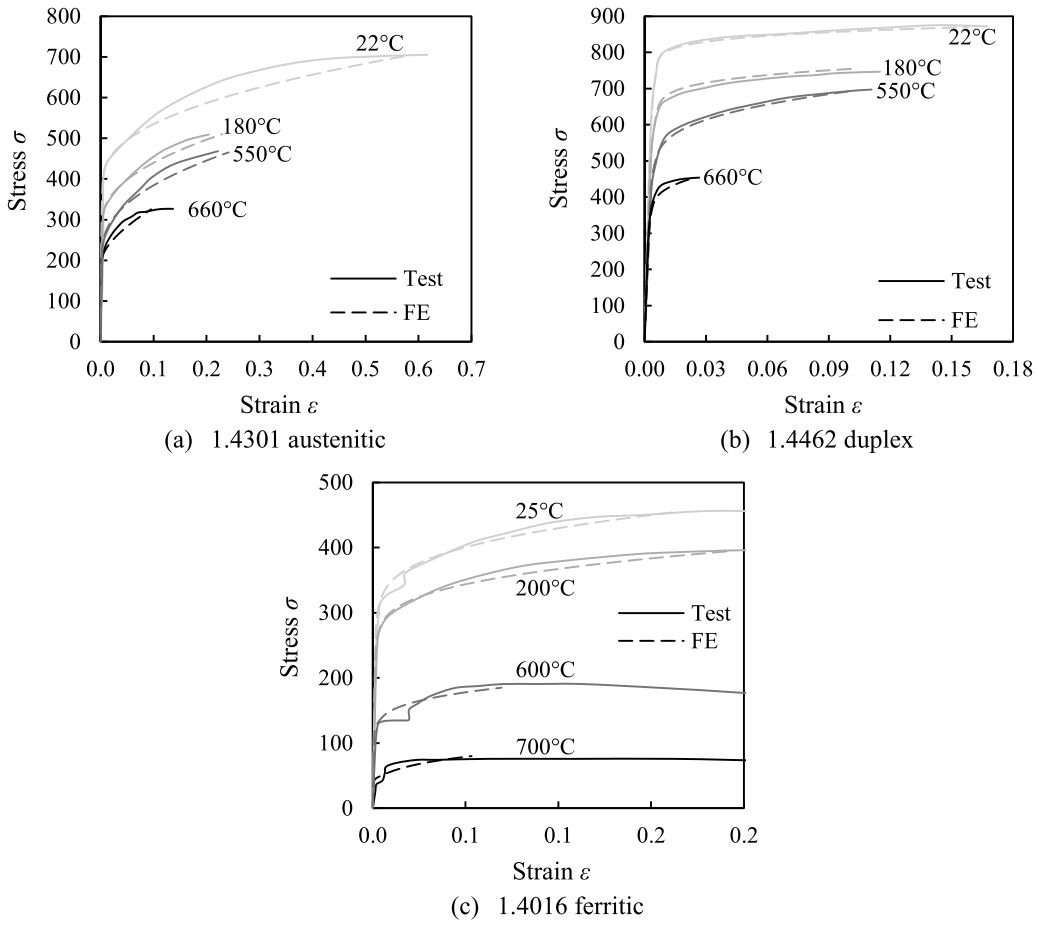

Fig. 4. Comparison of stress–strain curves predicted using the adopted material model against test results for austenitic, duplex [28] and ferritic [29] stainless steel.

Table 1
Overview of the adopted material properties in the FE models [34].

Type	Grade	Young's modulus E (N/mm^2)	Yield (0.2% proof) stress f_y (N/mm^2)	Ultimate stress f_u (N/mm^2)	Ultimate strain ε_u	Strain hardening exponent n
Cold-formed stainless steel SHS/RHS (flat regions)	Austenitic (A)	200000	460	700	0.20	7.1
	Duplex (D)		630	780	0.13	7.5
	Ferritic (F)		430	490	0.06	11.5
Cold-formed stainless steel SHS/RHS (corner regions)	Austenitic (A)	200000	640	830	0.20	6.4
	Duplex (D)		800	980	0.03	6.1
	Ferritic (F)		560	610	0.01	5.7
Hot-rolled stainless steel SHS/RHS	Austenitic (A)	200000	280	580	0.50	9.1
	Duplex (D)		530	770	0.30	9.3
	Ferritic (F)		320	480	0.16	17.2

be maintained at elevated temperatures (up to 700 °C). The upcoming version of the European structural steel fire design standard prEN 1993-1-2 [10] also recommends the use of the elevated temperature material reduction factors with the enhanced material strengths for cold-formed stainless steel cross-sections.

In line with the recommendations of [30], the strain hardening exponents n_θ used to define the roundedness of the first stages of the elevated temperature material response were taken equal to the room temperature values n, which are shown in Table 1 as provided in [34]. The strain hardening exponents m_θ defining the roundedness of the second stages of the elevated temperature material behaviour were determined through Eq. (4) [10], thereby ensuring that the second stages of the Ramberg–Osgood material model exactly pass through (i) the elevated temperature material strengths at 2% total strain $f_{2,\theta}$ at $\varepsilon_{2,\theta} = 0.02$ (i.e. 2% total strain) and (ii) the elevated temperature ultimate strengths $f_{u,\theta}$ at the elevated temperature ultimate strains $\varepsilon_{u,\theta}$, respectively.

$$m_\theta = \frac{\ln\left(\dfrac{0.02 - \varepsilon_{p0.2,\theta} - \frac{f_{2,\theta} - f_{p0.2,\theta}}{E_{p0.2,\theta}}}{\varepsilon_{u,\theta} - \varepsilon_{p0.2,\theta} - \frac{f_{u,\theta} - f_{p0.2,\theta}}{E_{p0.2,\theta}}}\right)}{\ln\left(\dfrac{f_{2,\theta} - f_{p0.2,\theta}}{f_{u,\theta} - f_{p0.2,\theta}}\right)} \text{ but } 1.5 \le m_\theta \le 5 \tag{4}$$

The room temperature and elevated temperature material stress–strain curves employed for the flat portions of cold-formed stainless steel SHS/RHS are shown in Fig. 3. Using the same material model and elevated temperature material reduction factors but with different room temperature material properties as provided in Table 1, the stress–strain curves for hot-rolled stainless steel SHS/RHS and corner regions of cold-formed stainless steel SHS/RHS could also be obtained. In Fig. 4, the adopted elevated temperature material stress–strain curves are

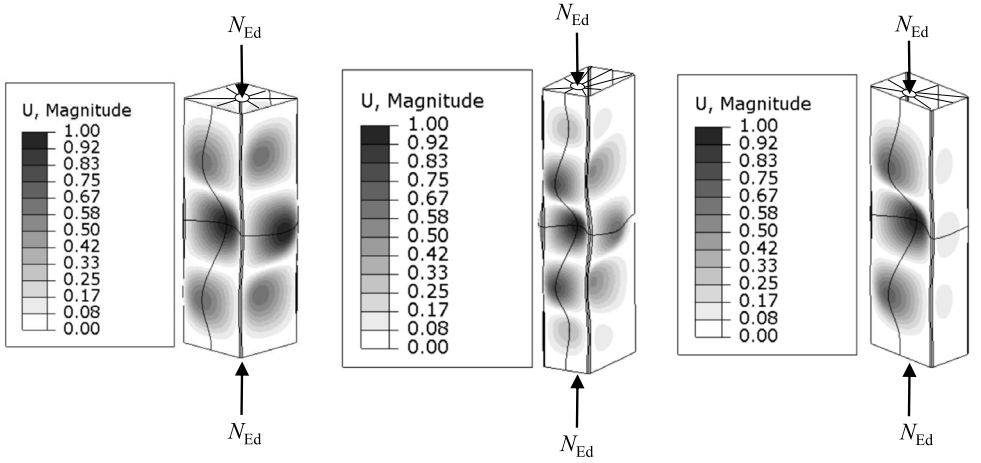

(a) SHS stub column under compression (b) RHS stub beam-column under combined compression and major axis bending (c) RHS stub beam-column under combined compression and minor axis bending

Fig. 5. Typical elastic local buckling modes of SHS and RHS stub column and stub beam–column.

compared against the results from the elevated temperature material tests on grade 1.4301 austenitic and grade 1.4462 duplex stainless steel coupons performed in [28] and grade 1.4016 ferritic stainless steel coupons carried out in [29]; correspondingly, the tested material properties of the coupons were utilised to generate the corresponding stress–strain curves using the adopted material model. It can be seen from Fig. 4 that the adopted material modelling is generally able to represent the elevated temperature material response of stainless steel coupons obtained from the elevated temperature material tests. As also previously indicated, the adopted material modelling approach in this paper (i.e. the two-stage Ramberg–Osgood material model and elevated temperature material reduction factors) will be incorporated into the upcoming version of EN 1993-1-2 [3]; thus, the elevated temperature material modelling approach of this study is completely in accordance with the recommendations of the upcoming version of the European structural steel fire design standard EN 1993-1-2 [3].

2.1.3. Initial imperfections

Since this study focuses on the behaviour and design of stainless steel cross-sections at elevated temperatures, global imperfections were not considered and only local geometric imperfections were taken into account in the parametric studies. Local geometric imperfections were incorporated into the FE models in the form of the lowest elastic local buckling modes obtained from the Linear Buckling Analyses (LBA) of the models. Fig. 5 presents examples of typical elastic local buckling modes obtained from LBA for (a) an SHS subjected to pure axial compression, (b) an RHS subjected to combined axial compression and major axis bending and (c) an RHS subjected to combined axial compression and minor axis bending. In accordance with the recommendations provided in Annex C of EN 1993-1-5 [38], the local imperfection amplitudes were taken as 80% of the geometric fabrication tolerances provided in EN 10219-2 [21] for cold-formed stainless steel SHS and RHS and EN 10210-2 [22] for hot-rolled stainless steel SHS and RHS. Thus, the local geometric imperfection magnitudes $e_{0,loc}$ for SHS and RHS were taken as 80% of $b_{cr}/100$, where b_{cr} is the overall width of the critical plate of an SHS or RHS in which the greatest normalised displacement was observed in the local buckling mode (i.e. $e_{0,loc} = 0.8(b_{cr}/100)$) in accordance with [39].

In [7], it was observed that residual stresses have negligible influence on the ultimate resistances of steel plates at elevated temperatures as they dissipate due to the development of thermal strains at elevated temperatures; [8,9] also made similar observations and did not include residual stresses in their numerical studies in the development of new effective width equations for the design of stainless steel and carbon steel plates and cross-sections at elevated temperatures. For hot-rolled stainless steel cross-sections, both membrane and bending residual stresses are shown to be negligible [14]. For cold-formed stainless steel SHS/RHS, the influence of the membrane residual stresses is also low as stated in [14,40] and the influence of the bending residual stresses is implicitly incorporated into the stress–strain curves derived considering the material tests performed on coupons that are cut from cold-formed stainless steel cross-sections [40]. This study adopted the elevated temperature material models obtained by applying material reduction factors to the standardised room temperature material properties for stainless steel cross-sections recommended in [38], which were derived based on the analysis of a comprehensive database of material tests on coupons extracted from various stainless steel products, thus taking into account the influence of the bending residual stresses within cold-formed stainless steel cross-sections. Thus, in line with previous studies [12,13], residual stresses were not included in the finite element models of stainless steel SHS and RHS in this paper.

2.2. Verification of numerical models

The shell FE models developed in this study were verified against the results from the fire experiments on stainless steel SHS and RHS stub columns and beams carried out in [41,42] and steel RHS beam–columns carried out in [43]. The geometric and material properties and the boundary and loading conditions of the shell FE models of the specimens created in the studies were consistent with those employed in the fire tests of [41–43]. The finite element models were also heated in accordance with the temperature development histories of the specimens reported in [41–43].

In Uppfeldt et al. [41], six anisothermal tests on austenitic stainless steel SHS stub columns were conducted, whereby prescribed axial loads were first applied to the specimens and then the temperatures of the specimens were increased up to failure while keeping the applied axial loading constant during the heating. The member lengths L and comparisons between the numerically determined critical temperatures θ_{FE} and the critical temperatures observed in the fire tests of [41] θ_{test} are shown in Table 2. The developed shell FE models were also verified against the anisothermal test performed in Gardner and Baddoo [42] on one austenitic stainless steel RHS beam with three faces exposed to fire; comparison between the numerically determined critical temperature

Table 2
Comparison of the critical temperatures obtained from the shell FE models θ_{FE} against those observed in the anisothermal fire experiments of Uppfeldt et al. [41] and Gardner and Baddoo [42] θ_{test}.

Reference	Test	Grade	Section	Member type	L mm	θ_{test} °C	θ_{FE} °C	$\theta_{FE}/\theta_{test}$
Uppfeldt et al. [41]	150 × 150×3–1	A	SHS	Stub column	900	676	712	1.053
	150 × 150×3–2				900	720	763	1.060
	150 × 150×3–3				900	588	575	0.978
	200 × 200×3–1				900	609	490	0.805
	200 × 200×3–2				900	685	651	0.950
	200 × 200×3–3				900	764	739	0.967
Gardner and Baddoo [42]	200 × 125×6	A	RHS	Beam	4400	884	919	1.039
Mean								0.979
CoV								0.084
Max								1.060
Min								0.805

Table 3
Comparison of the ultimate resistances of steel beam–columns obtained from the shell FE models $N_{u,FE}$ against those obtained from isothermal tests of Pauli et al. [43] $N_{u,test}$.

Reference	Test	Grade	Section	Member type	L mm	θ °C	$N_{u,test}$ kN	$N_{u,FE}$ kN	$N_{u,FE}/N_{u,test}$
Pauli et al. [43]	RHS120_SL_20C_z10	S355	RHS	Beam–column	1840	20	211	207.9	0.985
	RHS120_SL_20C_z50				1840	20	102	105.9	1.038
	RHS120_SL_400C_z10				1840	400	139	135.1	0.972
	RHS120_SL_400C_z50				1840	400	73	73.0	1.000
	RHS120_M_550C_z30				850	550	96	92.3	0.961
	RHS120_SL_550C_z10				1840	550	111	104.0	0.937
	RHS120_SL_550C_z50				1840	550	49	49.8	1.017
Mean									0.987
CoV									0.035
Max									1.038
Min									0.937

θ_{FE} and the critical temperature observed in the fire test of [42] θ_{test} is shown in Table 2 for the tested specimen. Note that the critical temperatures of the specimens of [41] and [42] were determined on the basis of the failure criteria for deformation and the rate of deformation provided in the European standard for the fire testing of structural elements EN 1363-1 (2012) [44]. Table 2 also shows a summary of the verification results compared against the experiments of [41,42] with the mean, coefficient of variation (CoV), maximum and minimum values of the ratios of the critical temperatures obtained from the shell FE models θ_{FE} to those observed in the fire experiments θ_{test} (i.e. $\theta_{FE}/\theta_{test}$). As can be seen from Table 2, the developed shell FE models are able to provide critical temperature predictions θ_{FE} that are close to the critical temperatures of the specimens θ_{test} observed in the fire experiments of [41] and [42].

Additionally, the developed shell FE models were also verified against seven isothermal tests performed in Pauli et al. [43] on steel RHS beam–columns. Table 3 summarises the mean, CoV, maximum and minimum values of the ratios of the ultimate resistances obtained from the shell FE models $N_{u,FE}$ to those obtained from the isothermal tests $N_{u,test}$(i.e. $N_{u,FE}/N_{u,test}$) for considered seven steel beam–columns at different temperatures θ. As can be seen from Table 3, the resistance predictions obtained from the developed shell FE models are close to those obtained from the isothermal tests in [43]. Fig. 6 also presents the experimental and numerical load–displacement curves for two tested specimens. As can be seen from the figure, the numerical load–displacement curves generally agree well with the experimental curves.

The FE verification carried out in this subsection indicates that the finite element modelling approach employed in this paper is able to accurately replicate the behaviour of stainless steel SHS and RHS at elevated temperatures and can be used in further parametric studies to generate benchmark structural performance data, against which the new design proposals for the fire design of stainless steel SHS/RHS can be assessed. Note that the finite element modelling approach adopted in this paper has also been extensively verified previously in [9,11,15,45] for stainless steel plates, cross-sections, columns and beams at elevated temperatures.

2.3. Parametric studies

Upon the verification of the adopted FE modelling approach, parametric studies were carried out on stainless steel SHS and RHS at elevated temperatures to generate comprehensive structural performance data on the behaviour of stainless steel SHS and RHS at elevated temperatures. In the parametric studies, various cross-section geometries and cross-section slendernesses, different loading conditions, various elevated temperature levels and different stainless steel grades were taken into consideration.

Tables 4 and 5 summaries the parameters taken into consideration in the numerical parametric studies performed on stainless steel SHS and RHS at elevated temperatures. Both cold-formed and hot-rolled austenitic, duplex and ferritic stainless steel SHS and RHS were considered, taking into account the structural response of (i) stub columns subjected to pure axial compression N_{Ed}, (ii) beams subjected to uniform major or minor axis bending M_{Ed}, (iiii) stub beam–columns subjected to combined axial compression and major or minor axis bending (N_{Ed}+M_{Ed}) and (iv) beams subjected to major or minor axis 3-point bending leading to the application of combined major or minor axis bending and shear (M_{Ed}+V_{Ed}). Isothermal analyses were performed on the considered stainless steel SHS and RHS members, adopting five different elevated temperature levels taken equal to 300 °C, 400 °C, 500 °C, 600 °C and 700 °C.

In the parametric studies, the overall cross-section depths h of SHS and RHS were taken as a constant value equal to 100 mm in all the considered cases. The aspect ratios of the stainless steel RHS, i.e. the cross-section depth h to width b ratios, were taken equal to 1.25, 1.67 and 2. Cross-section properties of SHS and RHS are shown in

Table 4
Summary of parametric studies on cold-formed and hot-rolled stainless steel SHS at elevated temperatures.

Material	θ (°C)	Cross-section slenderness				L/h			
		N_{Ed}	M_{Ed}	N_{Ed} + M_{Ed}	M_{Ed} + V_{Ed}	N_{Ed}	M_{Ed}	N_{Ed} + M_{Ed}	M_{Ed} + V_{Ed}
Cold-formed and hot-rolled A D F	300 400 500 600 700	$\bar{\lambda}_{p,H,c}$ = 0.2-2 with Δ0.2		$\bar{\lambda}_{p,H,c}$ = 0.2-2 with Δ0.3	$(h\text{-}2t)/(t\sqrt{\frac{235}{f_{y,flat}}})$ = $15/\eta$ - $55/\eta$ with $\Delta 10/\eta$	3	10	3	2, 3, 5, 10

Table 5
Summary of parametric studies on cold-formed and hot-rolled stainless steel RHS at elevated temperatures.

Material	θ (°C)	h/b	Cross-section slenderness				L/h			
			N_{Ed}	M_{Ed}	N_{Ed} + M_{Ed}	M_{Ed} + V_{Ed}	N_{Ed}	M_{Ed}	N_{Ed} + M_{Ed}	M_{Ed} + V_{Ed}
Cold-formed and hot-rolled A D F	300 400 500 600 700	1.25 1.67 2	$\bar{\lambda}_{p,H,c}$ = 0.2-2 with Δ0.2		$\bar{\lambda}_{p,H,c}$ = 0.2-2 with Δ0.3	$(h\text{-}2t)/(t\sqrt{\frac{235}{f_{y,flat}}})$ = $15/\eta$ - $55/\eta$ with $\Delta 10/\eta$ (major axis) $(b\text{-}2t)/(t\sqrt{\frac{235}{f_{y,flat}}})$ = $15/\eta$ - $55/\eta$ with $\Delta 10/\eta$ (minor axis)	3	10	3	L/h = 2, 3, 5, 10 (major axis) L/b = 2, 3, 5, 10 (minor axis)

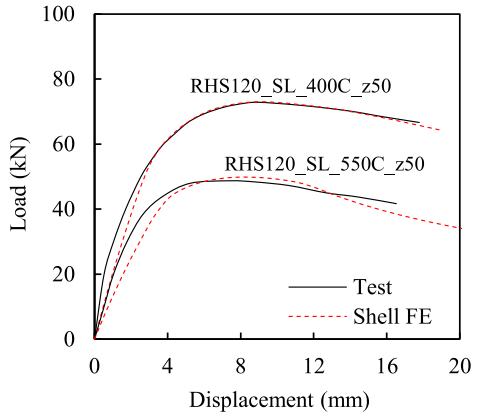

Fig. 6. Comparison of the load–displacement curves obtained from the isothermal tests in [43] and shell FE models for steel RHS beam–columns.

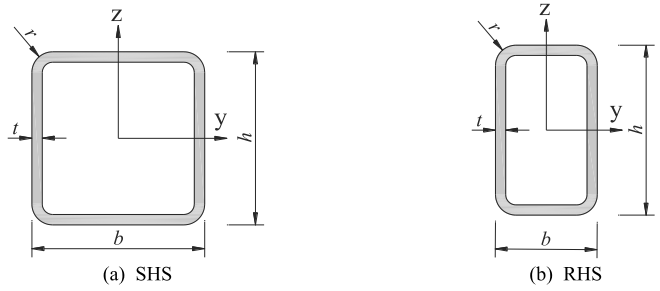

Fig. 7. Cross-section properties of SHS and RHS.

Fig. 7. For the considered stainless steel SHS and RHS, the cross-section thicknesses were varied such that the plate slendernesses of the flat portions of the stainless steel SHS and the wider flat portions of the stainless steel RHS determined considering the pure axial compression loading case $\bar{\lambda}_{p,H,c}$ ranged from (i) 0.2 to 2 with an increment of 0.2 for the stub columns and beams and (ii) 0.2 to 2 with an increment of 0.3 for the stub beam–columns. For the case of the stainless steel SHS elements subjected to three-point bending (i.e. combined bending and shear) and the stainless steel RHS elements subjected to major axis three-point bending (i.e. combined major axis bending and shear), the cross-section thicknesses were varied through considering the non-dimensional parameter $(h\text{-}2t)/(t\sqrt{235/f_{y,flat}})$ which ranged between $15/\eta$ and $55/\eta$ with an increment of $10/\eta$, where η is the auxiliary coefficient taken as 1.2 and $f_{y,flat}$ is (i) the room temperature 0.2% proof strength for a hot-rolled SHS/RHS and (ii) the room temperature 0.2% proof strength of the flat regions for a cold-formed SHS/RHS. On the other hand, for the stainless steel RHS elements subjected to minor axis three-point bending (i.e. combined minor axis bending and shear), the cross-section thicknesses were varied by changing the non-dimensional parameter $(b\text{-}2t)/(t\sqrt{235/f_{y,flat}})$ between $15/\eta$ and $55/\eta$ with an increment of $10/\eta$. Note that the non-dimensional parameters $(h\text{-}2t)/(t\sqrt{235/f_{y,flat}})$ and $(b\text{-}2t)/(t\sqrt{235/f_{y,flat}})$ were used in the variations of the cross-section thicknesses for the stainless steel SHS and RHS subjected to combined bending and shear in this paper, taking into account that EN 1993-1-4 [3] specifies $(h\text{-}2t)/(t\sqrt{235/f_{y,flat}}) = 56.2/\eta$ and $(b\text{-}2t)/(t\sqrt{235/f_{y,flat}}) = 56.2/\eta$ as the shear buckling limits with $\eta = 1.2$ for SHS and RHS, below which shear buckling can be neglected. This study did not explore the shear buckling of SHS and RHS at elevated temperatures, which will be comprehensively investigated in future research. In EN 1993 – 1 – 4 [5], the nominal thicknesses of cold-formed stainless steel cross-sections are limited to 6.4 mm or 8 mm for different grades. Thus, the cross-section thicknesses of the cold-formed stainless steel SHS/RHS investigated in this paper were limited to 6 mm in the numerical parametric studies in line with [46].

For the stainless steel SHS and RHS stub columns and stub beam–columns, the member lengths L were taken as three times of the cross-section depths h (i.e. $L = 3h$) in accordance with [47], which are deemed short enough to avoid the influence of global buckling but also long enough to allow the free development of local buckling. On the other hand, for the stainless steel SHS and RHS subjected to pure bending, the member lengths L were taken as ten times of the cross-section depths (i.e. $L = 10h$). In the case of the stainless steel SHS and RHS members subjected to 3-point bending (combined bending and shear), to capture different interaction levels of bending and shear,

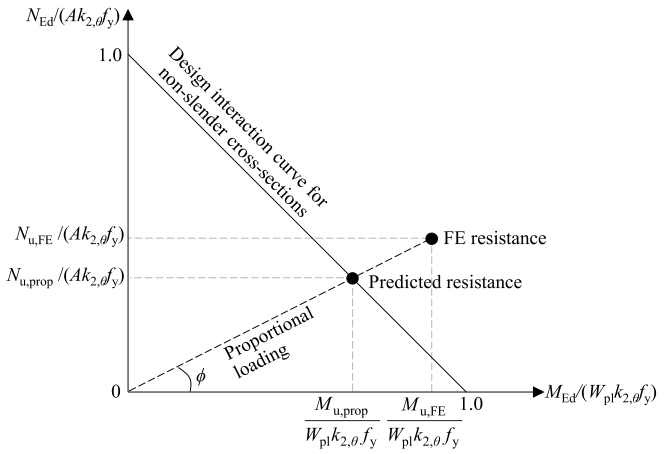

Fig. 8. Definition of radial angle ϕ for the combined compression and bending loading condition.

different member lengths were adopted. For the stainless steel SHS and RHS members subjected to major axis 3-point bending, the member length to cross-section depth ratios L/h were taken as 2, 3, 5, and 10 (i.e. L/h = 2, 3, 5 and 10). For the stainless steel RHS members subjected to minor axis 3-point bending, the member length to cross-section width ratios L/b were taken as 2, 3, 5, and 10 (i.e. L/b = 2, 3, 5 and 10).

In this study, a parameter referred to as the radial angle ϕ was adopted to describe the interaction levels between the applied axial compression N_{Ed} and bending moments M_{Ed} for the stainless steel SHS and RHS stub beam–columns as determined by Eq. (5) and presented in Fig. 8. Note that in Eq. (5) and Fig. 8, A and W_{pl} are the cross-section area and plastic section modulus, respectively.

$$\phi = \tan^{-1}\left(\frac{N_{Ed}/(Ak_{2,\theta}f_y)}{M_{Ed}/(W_{pl}k_{2,\theta}f_y)}\right) \tag{5}$$

As shown in Fig. 8, the radial angle ϕ varies between 0° and 90°. In this study, in addition to pure bending ϕ = 0° and pure axial compression ϕ = 90°, five different radial angles ϕ equal to 15°, 30°, 45°, 60° and 75° were adopted in the parametric studies so as to investigate the behaviour of stainless steel SHS and RHS stub beam–columns subjected to various intensities of axial compression and bending moments at elevated temperatures. Note that in the determination of the radial angles ϕ through Eq. (5), f_y was taken as the average 0.2% proof strengths $f_{y,ave}$ of the cold-formed stainless steel SHS and RHS calculated considering the enhanced material strengths in the corner regions in this study. The determination of $f_{y,ave}$ is discussed in Section 3.1.

In the extensive numerical parametric studies performed in this subsection, (i) 1140 stainless steel SHS and RHS stub columns, (ii) 1995 stainless steel SHS and RHS beams subjected to pure bending, (iii) 6825 stainless steel SHS and RHS stub beam–columns and (iv) 3900 stainless steel SHS and RHS beams under three-point bending (combined bending and shear) were taken into consideration. In total, 13860 stainless steel SHS and RHS elements at elevated temperatures were considered in the numerical parametric studies conducted in this paper, which generated very extensive benchmark structural performance data on the behaviour of stainless steel SHS and RHS at elevated temperatures. This comprehensive structural performance data will be utilised in the following sections for the assessment of the existing design rules of EN 1993-1-2 [3] and the proposed design method for stainless steel SHS and RHS structural elements at elevated temperatures.

3. EN 1993-1-2 fire design method for stainless steel SHS and RHS

In this section, the methods provided in the European structural steel fire design standard EN 1993-1-2 [3] for the design of stainless steel SHS and RHS at elevated temperatures are briefly introduced. The accuracy of EN 1993-1-2 for the design of stainless steel SHS and RHS at elevated temperatures is assessed in Section 5.

3.1. Cross-section classification

For the classification of stainless steel cross-sections at elevated temperatures, EN 1993-1-2 [3] recommends the use of the cross-section classification rules provided in the European room temperature structural stainless steel design standard EN 1993-1-4 [5] but with a reduced material factor at elevated temperature ε_θ which is given by Eq. (6) where ε is the room temperature material factor.

$$\varepsilon_\theta = 0.85\varepsilon = 0.85\sqrt{\frac{235}{f_y}\frac{E}{210000}} \tag{6}$$

In accordance with EN 1993-1-4 [5], stainless steel SHS and RHS at elevated temperatures are classified into four classes on the basis of the width-to-thickness ratios of the constituent plates within the cross-sections. Table 6 summarises the limit width-to-thickness ratios for internal and outstand stainless steel cross-section elements at elevated temperatures in accordance with the recommendations of EN 1993-1-2 [3] and EN 1993-1-4 [5]. Note that according to the UK National Annex [48] to EN 1993-1-4 [5], the cross-section resistances of cold-formed stainless steel SHS and RHS can be determined using the average room temperature 0.2% proof strengths $f_{y,ave}$ of the cross-sections, taking into account the enhanced material strengths in the corner regions. The average room temperature 0.2% proof strength of a cold-formed SHS/RHS $f_{y,ave}$ can be calculated as [30]:

$$f_{y,ave} = \frac{f_{y,corner}A_{corner} + f_{y,flat}\left(A - A_{corner}\right)}{A} \tag{7}$$

in which $f_{y,corner}$ and $f_{y,flat}$ are the room temperature 0.2% proof strengths within the corner regions and flat regions respectively and A_{corner} is the total corner area including the extensions into the flat regions equal to two times of the cross-section thickness t. Note that Eq. (7) can be utilised for cold-formed stainless steel SHS/RHS subjected to all types of loading conditions (i.e. compression, bending and combined bending and compression) in accordance with the recommendations of the Steel Construction Institute (SCI) Design Manual for Structural Stainless Steel [30]; the next revision of EN 1993-1-4 [5] also explicitly states this recommendation, including Eq. (7) for the determination of $f_{y,ave}$.

The cross-section resistances of cold-formed stainless steel SHS/RHS at elevated temperatures can be determined through the elevated temperature material strengths $f_{2,\theta}$ and $f_{p0.2,\theta}$ calculated by reducing the average 0.2% proof strengths $f_{y,ave}$ of the cross-sections; in this case, the cross-section classification of cold-formed stainless steel SHS/RHS at elevated temperatures should be carried out using the elevated temperature material factor $\varepsilon_{ave,\theta}$ based on $f_{y,ave}$ as determined by Eq. (8), which is in line with the method recommended in the upcoming version of EN 1993-1-4 [5] for the determination of the room temperature material factor ε_{ave}.

$$\varepsilon_{ave,\theta} = 0.85\varepsilon_{ave} = 0.85\sqrt{\frac{235}{f_{y,ave}}\frac{E}{210000}} \tag{8}$$

3.2. Cross-section resistance

3.2.1. Pure axial compression and pure bending

According to EN 1993-1-2 [3], the cross-section resistances of stainless steel structural elements at elevated temperatures are determined as shown in Table 7 for different cross-section classes. In Table 7,

Table 6
Width-to-thickness limits for the classification of stainless steel plates at elevated temperatures according to EN 1993-1-2 [3].

Element	Class 1	Class 2	Class 3
Internal element under compression	$33\varepsilon_\theta$	$35\varepsilon_\theta$	$37\varepsilon_\theta$
Internal element under bending	$72\varepsilon_\theta$	$76\varepsilon_\theta$	$90\varepsilon_\theta$
Outstand element under compression	$9\varepsilon_\theta$	$10\varepsilon_\theta$	$14\varepsilon_\theta$

Table 7
Cross-section resistances of SHS and RHS at elevated temperatures according to EN 1993-1-2 [3].

Class	Compression	Bending
Class 1 and 2	$N_{\mathrm{fi,t,Rd}} = Ak_{2,\theta}f_{\mathrm{y}}/\gamma_{\mathrm{M,fi}}$	$M_{\mathrm{fi,t,Rd}} = W_{\mathrm{pl}}k_{2,\theta}f_{\mathrm{y}}/\gamma_{\mathrm{M,fi}}$
Class 3	$N_{\mathrm{fi,t,Rd}} = Ak_{2,\theta}f_{\mathrm{y}}/\gamma_{\mathrm{M,fi}}$	$M_{\mathrm{fi,t,Rd}} = W_{\mathrm{el}}k_{2,\theta}f_{\mathrm{y}}/\gamma_{\mathrm{M,fi}}$
Class 4	$N_{\mathrm{fi,t,Rd}} = A_{\mathrm{eff}}k_{\mathrm{p0.2},\theta}f_{\mathrm{y}}/\gamma_{\mathrm{M,fi}}$	$M_{\mathrm{fi,t,Rd}} = W_{\mathrm{eff}}k_{\mathrm{p0.2},\theta}f_{\mathrm{y}}/\gamma_{\mathrm{M,fi}}$

$N_{\mathrm{fi,t,Rd}}$ and $M_{\mathrm{fi,t,Rd}}$ are the design cross-section axial compression and bending moment resistances for temperature θ at time t, A and A_{eff} are the full and effective cross-section areas, W_{pl}, W_{el} and W_{eff} are the plastic, elastic and effective section moduli and $\gamma_{\mathrm{M,fi}}$ is the partial safety factor for fire design equal to unity. According to EN 1993-1-2 [3], the effective cross-section properties A_{eff} and W_{eff} at elevated temperatures should be taken the same as those for room temperature design. Thus, the effective cross-section properties A_{eff} and W_{eff} are calculated through the effective width method provided in EN 1993-1-4 [5] by reducing the widths of the slender constituent plates through local buckling reduction factors ρ, which are determined by means of Eq. (9) for internal elements and Eq. (10) for outstand elements.

$$\rho = \frac{0.772}{\bar{\lambda}_{\mathrm{p}}} - \frac{0.079}{\bar{\lambda}_{\mathrm{p}}^{\,2}} \text{ but } \rho \le 1.0 \tag{9}$$

$$\rho = \frac{1}{\bar{\lambda}_{\mathrm{p}}} - \frac{0.188}{\bar{\lambda}_{\mathrm{p}}^{\,2}} \text{ but } \rho \le 1.0 \tag{10}$$

In Eqs. (9) and (10), $\bar{\lambda}_{\mathrm{p}}$ is the room temperature non-dimensional plate slenderness given by Eq. (11)

$$\bar{\lambda}_{\mathrm{p}} = \sqrt{\frac{f_{\mathrm{y}}}{\sigma_{\mathrm{cr}}}} \tag{11}$$

where σ_{cr} is the elastic local buckling stress of the plate (i.e. flange or web) determined through Eq. (12).

$$\sigma_{\mathrm{cr}} = k_\sigma \frac{\pi^2 E}{12\left(1-\upsilon^2\right)}\left(\frac{t}{b}\right)^2 \tag{12}$$

In Eq. (12), E is the Young's modulus, υ is the Poisson's ratio equal to 0.3 (i.e. $\upsilon = 0.3$), b and t are the plate width and thickness and k_σ is the plate buckling coefficient determined in accordance with the European design standard for plated structural elements EN 1993-1-5 [38] on the basis of the edge boundary and loading conditions of the plate.

As shown in Table 7, according to EN 1993-1-2 [3], (i) the elevated temperature material strengths at 2% total strain $f_{2,\theta} = k_{2,\theta}f_{\mathrm{y}}$ should be used as the reference material strengths in the determination of the ultimate resistances of Class 1, 2 and 3 cross-sections at elevated temperatures and (ii) the elevated temperature 0.2% proof strengths $f_{\mathrm{p0.2},\theta} = k_{\mathrm{p0.2},\theta}f_{\mathrm{y}}$ should be used as the reference material strengths in the determination of the ultimate resistances of Class 4 cross-sections at elevated temperatures. Thus, there is an artificial step between the ultimate resistance predictions between Class 3 and Class 4 cross-sections at elevated temperatures according to the provisions of EN 1993-1-2 [3].

As previously indicated, for the determination of the cross-section resistances $N_{\mathrm{fi,t,Rd}}$ and $M_{\mathrm{fi,t,Rd}}$ of cold-formed stainless steel SHS and RHS at elevated temperatures, the average room temperature 0.2% proof strengths of the cross-sections $f_{\mathrm{y,ave}}$ calculated as given by Eq. (7) and taking into account the enhanced material strengths in the corner regions can be used in accordance with the UK National Annex [48] to EN 1993-1-4 [5] and the Steel Construction Institute (SCI) Design Manual for Structural Stainless Steel [30]. In this case, the average room temperature 0.2% proof strengths of cold-formed stainless steel SHS/RHS $f_{\mathrm{y,ave}}$ are reduced through the corresponding material reduction factors $k_{2,\theta}$ and $k_{\mathrm{p0.2},\theta}$ to determine the elevated temperature material strengths at 2% total strain $f_{2,\theta} = k_{2,\theta}f_{\mathrm{y,ave}}$ and the elevated temperature 0.2% proof strengths $f_{\mathrm{p0.2},\theta} = k_{\mathrm{p0.2},\theta}f_{\mathrm{y,ave}}$ in the cross-section fire design. If the elevated temperature material strengths $f_{2,\theta}$ and $f_{\mathrm{p0.2},\theta}$ determined through the average room temperature 0.2% proof strengths of the cross-sections $f_{\mathrm{y,ave}}$ are adopted for the fire design of cold-formed stainless steel SHS and RHS, the room temperature 0.2% proof strengths f_{y} given in Eq. (11) and Table 7 should be replaced by $f_{\mathrm{y,ave}}$ in the determination of the plate slendernesses $\bar{\lambda}_{\mathrm{p}}$ of the cross-section elements and the elevated temperature cross-section axial compression $N_{\mathrm{fi,t,Rd}}$ and bending moment $M_{\mathrm{fi,t,Rd}}$ resistances, respectively.

3.2.2. Combined axial compression and bending

EN 1993-1-2 [3] does not provide specific expressions for the design of stainless steel cross-sections subjected to combined compression and bending at elevated temperatures. Hence, in this study, the equations provided in EN 1993-1-2 [3] for the design of stainless steel beam–columns at elevated temperatures were employed for the design of stainless steel cross-sections under combined axial compression and bending at elevated temperatures, considering the cross-section design as an extreme case of beam–column design where the global instability effects are not of significance and disregarded. Thus, the global buckling reduction factors in the member design calculations provided in EN 1993-1-2 [3] were taken equal to unity and only the interaction between the cross-section axial compression $N_{\mathrm{fi,t,Rd}}$ and bending moment $M_{\mathrm{fi,t,Rd}}$ resistances was taken into consideration. The beam–column design equation of EN 1993-1-2 [3] used in this study for the ultimate cross-section strength predictions of SHS and RHS subjected to combined compression and bending at elevated temperatures is given by Eq. (13)

$$\frac{N_{\mathrm{Ed}}}{N_{\mathrm{fi,t,Rd}}} + \frac{k_{\mathrm{y}}M_{\mathrm{y,Ed}}}{M_{\mathrm{y,fi,t,Rd}}} + \frac{k_{\mathrm{z}}M_{\mathrm{z,Ed}}}{M_{\mathrm{z,fi,t,Rd}}} \le 1 \tag{13}$$

in which $M_{\mathrm{y,Ed}}$ and $M_{\mathrm{z,Ed}}$ are the applied major and minor axis first-order bending moments, $M_{\mathrm{y,fi,t,Rd}}$ and $M_{\mathrm{z,fi,t,Rd}}$ are the design major and minor axis bending resistances for temperature θ at time t and k_{y} and k_{z} are the interaction factors as given by Eqs. (14) and (15)

$$k_{\mathrm{y}} = 1 - \frac{\mu_{\mathrm{y}}N_{\mathrm{Ed}}}{N_{\mathrm{fi,t,Rd}}} \le 3, \text{ with } \mu_{\mathrm{y}} = \left(2\beta_{\mathrm{M,y}} - 5\right)\bar{\lambda}_{\mathrm{y},\theta} + 0.44\beta_{\mathrm{M,y}} + 0.29 \le 0.8 \tag{14}$$

$$k_{\mathrm{z}} = 1 - \frac{\mu_{\mathrm{z}}N_{\mathrm{Ed}}}{N_{\mathrm{fi,t,Rd}}} \le 3, \text{ with } \mu_{\mathrm{z}} = \left(1.2\beta_{\mathrm{M,z}} - 3\right)\bar{\lambda}_{\mathrm{z},\theta} + 0.71\beta_{\mathrm{M,z}} - 0.29 \le 0.8 \tag{15}$$

where $\beta_{\mathrm{M,y}}$ and $\beta_{\mathrm{M,z}}$ are the major and minor axis equivalent uniform moment factors which are equal to 1.1 for the uniform bending moment case (i.e $\beta_{\mathrm{M,y}} = 1.1$ and $\beta_{\mathrm{M,z}} = 1.1$). Since global buckling is disregarded in the determination of the cross-section strength predictions at elevated temperatures herein, the elevated temperature member slendernesses for in-plane buckling $\bar{\lambda}_{\mathrm{y},\theta}$ and out-of-plane buckling $\bar{\lambda}_{\mathrm{z},\theta}$ are taken equal to the extreme value of 0 in Eqs. (14) and (15).

3.2.3. Combined bending and shear

High shear effects have an adverse influence on the cross-section resistances of stainless steel members at both room temperature and elevated temperatures, which should be considered in their cross-section design. The European structural steel fire design standard EN 1993-1-2 [3] directs the designers to the European room temperature structural steel design standard EN 1993-1-1 [49] for the consideration of the influence of high shear on the cross-section resistances

of structural steel elements at elevated temperatures. Thus, for cross-sections subjected to high shear forces at elevated temperatures, the elevated temperature cross-section resistances should be reduced by using the reduced elevated temperature material strengths $f_{y,\theta,r}$ as given by Eq. (16), where $k_{y,\theta}$ is equal to $k_{2,\theta}$ for Class 1, 2 and 3 cross-sections and $k_{p0.2,\theta}$ for Class 4 cross-sections. In Eq. (16), f_y can be taken as $f_{y,ave}$ for cold-formed stainless steel SHS and RHS.

$$f_{y,\theta,r} = \left(1 - \rho_v\right) k_{y,\theta} f_y \tag{16}$$

In Eq. (16), ρ_v is a reduction factor which is used to reduce the elevated temperature material strength when the applied shear force V_{Ed} exceeds half of the elevated temperature plastic shear capacity $V_{fi,t,Rd}$ (i.e. $V > 0.5V_{fi,t,Rd}$) as given by Eq. (17). The elevated temperature plastic shear resistance $V_{fi,t,Rd}$ can be calculated using Eq. (18), in which A_v is the shear area and f_y is the yield strength of the flat regions. The shear area A_v can be determined through Eq. (19) for SHS and RHS.

$$\rho_v = (2V/V_{fi,t,Rd} - 1)^2 \text{ for} V > 0.5V_{fi,t,Rd} \tag{17}$$

$$V_{fi,t,Rd} = A_v k_{2,\theta} f_y/\sqrt{3} \tag{18}$$

$$A_v = \begin{cases} Ah/(b+h) \text{ for SHS and RHS under major axis} \\ \quad \text{bending and shear} \\ Ab/(b+h) \text{ for RHS under minor axis bending and shear} \end{cases} \tag{19}$$

4. New fire design proposals for stainless steel SHS RHS

In this section, the design rules of stainless steel SHS and RHS subjected to different loading conditions at elevated temperatures are developed, considering the plate fire design recommendations in [9]. It is important to note that this study recommends the use of the elevated temperature material strengths at 2% total strain $f_{2,\theta}$ calculated by reducing the average room temperature 0.2% proof strengths $f_{y,ave}$ (i.e. $f_{2,\theta} = k_{2,\theta} f_{y,ave}$) in the determination of the cross-section resistances of cold-formed stainless steel SHS and RHS at elevated temperatures, thereby taking into account the enhanced material strengths within the corner regions of cold-formed stainless steel SHS and RHS. Thus, in the cross-section fire design methods put forward in this paper, the reduction of the average room temperature 0.2% proof strengths $f_{y,ave}$ in lieu of the room temperature 0.2% proof strengths of the flat regions $f_{y,flat}$ is recommended in the determination of the cross-section resistances of cold-formed stainless steel SHS and RHS at elevated temperatures. In the case of hot-rolled stainless steel SHS and RHS, of course, the elevated temperature material strengths at 2% total strain $f_{2,\theta}$ calculated by reducing the room temperature 0.2% proof strengths uniform across the cross-sections f_y should be used in the determination of the ultimate cross-section resistances (i.e. $f_{2,\theta} = k_{2,\theta} f_y$). Thus, the reference room temperature 0.2% proof strengths f_y^* adopted and correspondingly reduced in the application of the proposed fire design methods in this paper can be determined as shown in Eq. (20). As previously introduced, the average room temperature 0.2% proof strength of a cold-formed stainless steel SHS/RHS $f_{y,ave}$ can be calculated as given by Eq. (7).

$$\begin{aligned} f_y^* &= f_{y,ave} \quad \text{for cold-formed SHS and RHS} \\ f_y^* &= f_y \quad \text{for hot-rolled SHS and RHS} \end{aligned} \tag{20}$$

It is worth noting that even though the consideration of the strength enhancements in the corner regions is recommended in the determination of the ultimate resistances of cold-formed stainless steel SHS/RHS at elevated temperatures in this study, these strength enhancements can be conservatively neglected and the material strengths within the flat portions of the cold-formed stainless steel SHS/RHS can be used in conjunction with the proposed design approach in the determination of the ultimate resistances of cold-formed stainless steel SHS/RHS at elevated temperatures.

4.1. Cross-section classification

In accordance with Xing et al. [9], this study recommends the replacement of the traditional EN 1993-1-2 cross-section classification system with a new cross-section classification framework, employing two distinct cross-section classes and categorising stainless steel cross-sections into (i) 'non-slender' and (ii) 'slender' classes at elevated temperatures. In the new cross-section classification framework, the class of a cross-section is specified by taking into account the class of its most slender constituent plate element. If the elevated temperature plate slenderness $\overline{\lambda}_{p,\theta}$ of a cross-section plate element is greater than the corresponding threshold slenderness $\overline{\lambda}_{p0,\theta}$, the cross-section element is classified as 'slender'. On the other hand, if the elevated temperature plate slenderness $\overline{\lambda}_{p,\theta}$ of a cross-section plate element is less than the threshold slenderness $\overline{\lambda}_{p0,\theta}$, the cross-section element is classified as 'non-slender'. If one or more cross-section plate elements of a stainless steel cross-section are classified as 'slender', the cross-section is classified as 'slender'. By contrast, if all the cross-section plate elements of a cross-section are classified as 'non-slender', the cross-section is classified as 'non-slender'. The elevated temperature plate slenderness $\overline{\lambda}_{p,\theta}$ of a cross-section element is determined by Eq. (21):

$$\overline{\lambda}_{p,\theta} = \xi_\theta \sqrt{\frac{f_y^*}{\sigma_{cr}}} \quad \text{with } \xi_\theta = \sqrt{\frac{k_{2,\theta}}{k_{E,\theta}}} \tag{21}$$

where σ_{cr} is the elastic critical buckling stress of the plate element (i.e. flange or web) at room temperature as determined through Eq. (22). In accordance with EN 1993-1-5 [38], the plate widths b of SHS and RHS in Eq. (22) are taken equal to the widths of the flat portions without the rounded corners.

$$\sigma_{cr} = k_\sigma \frac{\pi^2 E}{12\left(1-\nu^2\right)} \left(\frac{t}{b}\right)^2 \tag{22}$$

The threshold slenderness $\overline{\lambda}_{p0,\theta}$ used in the proposed approach is calculated by Eq. (23) for internal plate elements in austenitic stainless steel sections

$$\overline{\lambda}_{p0,\theta} = \left(0.27 + \sqrt{0.0279 - 0.015\psi}\right)^{1.33} \sqrt{\xi_\theta} \tag{23}$$

and by Eq. (24) for outstand flange plates in austenitic stainless steel sections.

$$\overline{\lambda}_{p0,\theta} = 0.237\sqrt{\xi_\theta} \tag{24}$$

On the other hand, the threshold slenderness $\overline{\lambda}_{p0,\theta}$ is determined through Eq. (25) for internal plate elements in duplex and ferritic stainless steel sections

$$\overline{\lambda}_{p0,\theta} = \left(0.3 + \sqrt{0.045 - 0.015\psi}\right)^{1.33} \sqrt{\xi_\theta} \tag{25}$$

and by Eq. (26) for outstand flange plates in duplex and ferritic stainless steel sections.

$$\overline{\lambda}_{p0,\theta} = 0.344\sqrt{\xi_\theta} \tag{26}$$

In Eqs. (23) and (25), $\psi = \sigma_2/\sigma_1$ is the ratio of the stresses at the two edges of the plate. Note that in accordance with EN 1993-1-5 [38], $\psi = \sigma_2/\sigma_1$ is determined by taking the ratio of the minimum compressive edge stress or tensile edge stress σ_2 to the maximum compressive edge stress σ_1 (with compression positive).

4.2. Cross-section resistance

4.2.1. Pure compression and pure bending

In the proposed cross-section fire design approach, the axial compression resistance $N_{fi,t,Rd}$ of a cross-section for temperature θ at time t is determined as given by Eqs. (27) and (28)

$$N_{fi,t,Rd} = \frac{Ak_{2,\theta} f_y^*}{\gamma_{M,fi}} \quad \text{for non-slender sections} \tag{27}$$

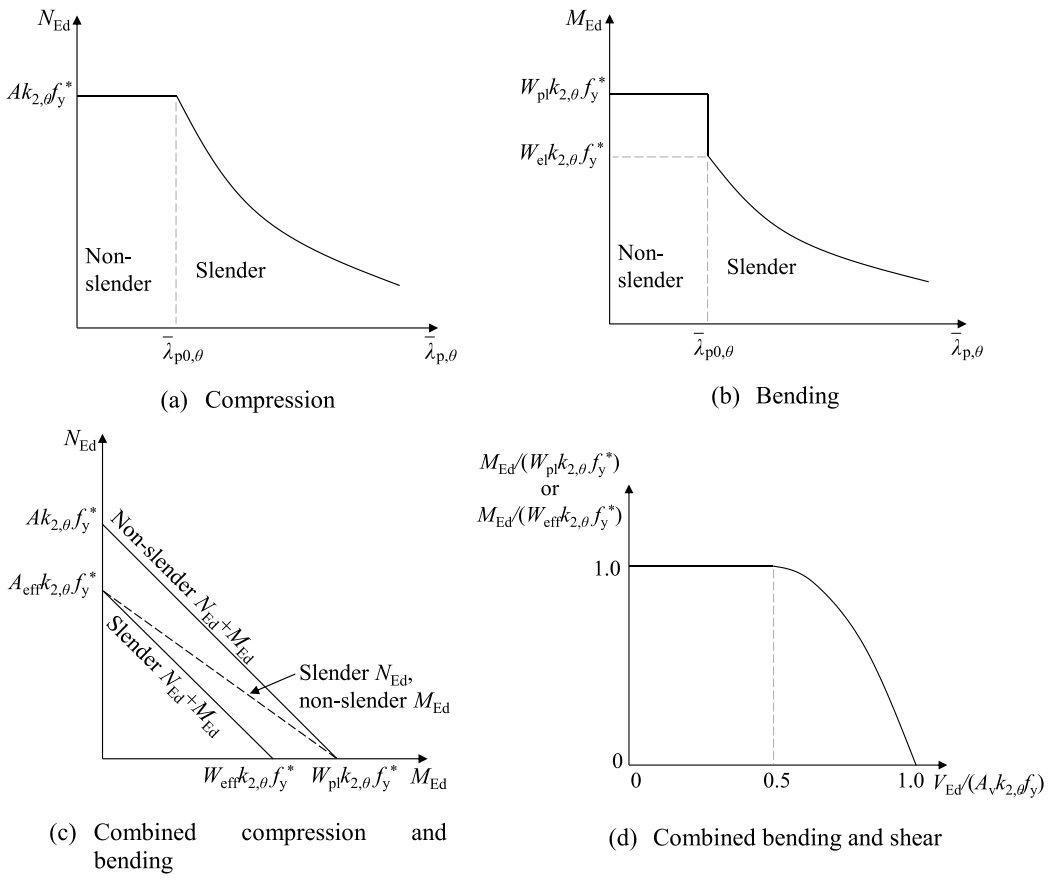

Fig. 9. Determination of design cross-section resistances of stainless steel SHS and RHS at elevated temperatures under different loading conditions in the proposed design method.

$$N_{fi,t,Rd} = \frac{A_{eff}k_{2,\theta}f_y^*}{\gamma_{M,fi}} \quad \text{for slender sections} \tag{28}$$

in which A and A_{eff} are the full and effective cross-section areas respectively. The bending moment resistance $M_{fi,t,Rd}$ of a cross-section for temperature θ at time t is calculated as

$$M_{fi,t,Rd} = \frac{W_{pl}k_{2,\theta}f_y^*}{\gamma_{M,fi}} \quad \text{for non-slender sections} \tag{29}$$

$$M_{fi,t,Rd} = \frac{W_{eff}k_{2,\theta}f_y^*}{\gamma_{M,fi}} \quad \text{for slender sections} \tag{30}$$

where W_{pl} and W_{eff} are the plastic and effective section moduli respectively. Table 8 also summarises the design resistance calculations recommended in this study for stainless steel SHS and RHS subjected to pure compression and pure bending at elevated temperatures. As illustrated in Table 8 and Fig. 9(a) and (b), different than the local buckling assessment rules of EN 1993-1-2, the elevated temperature material strengths at 2% total strain $f_{2,\theta} = k_{2,\theta}f_y^*$ are adopted as the reference material strengths in the determination of the ultimate cross-section resistances of stainless steel cross-sections regardless of their cross-section class. In line with the effective width method set out in EN 1993-1-5 [38], in the proposed cross-section fire design approach, the effective section properties A_{eff} and W_{eff} are determined on the basis of the effective widths of the slender constituent plates within the cross-sections; the effective width of a plate b_{eff} is calculated through the multiplication of the local buckling reduction factor ρ by the compressive plate width b_c as described in EN 1993-1-5 [38], i.e. $b_{eff} = \rho b_c$.

As previously indicated, the ultimate resistance predictions of stainless steel SHS and RHS at elevated temperatures are determined based on the effective width method established in [9] for stainless steel plates at elevated temperatures. Even though stainless steel SHS and RHS only involve internal cross-section elements, the effective width equations of [9] for outstand cross-section elements are also included herein for the sake of completeness. In accordance with the recommendations of [9], the local buckling reduction factor ρ is taken equal to unity for non-slender stainless steel cross-section plate elements at elevated temperatures as given by Eq. (31).

Table 8
Definition of the ultimate compression and bending moment resistances of SHS/RHS at elevated temperatures in the new proposed method in accordance with the design approach introduced in [9].

Classification	Compression	Bending
Non-slender	$N_{fi,t,Rd} = Ak_{2,\theta}f_y/\gamma_{M,fi}$	$M_{fi,t,Rd} = W_{pl}k_{2,\theta}f_y/\gamma_{M,fi}$
Slender	$N_{fi,t,Rd} = A_{eff}k_{2,\theta}f_y/\gamma_{M,fi}$	$M_{fi,t,Rd} = W_{eff}k_{2,\theta}f_y/\gamma_{M,fi}$

$$\rho = 1 \quad \text{for} \quad \bar{\lambda}_{p,\theta} \le \bar{\lambda}_{p0,\theta} \tag{31}$$

In the case of slender internal cross-section plate elements in austenitic stainless steel cross-sections, the local buckling reduction factor ρ is determined by Eq. (32).

$$\rho = \frac{0.54}{\left(\bar{\lambda}_{p,\theta}/\sqrt{\xi_\theta}\right)^{0.75}} - \frac{0.015\,(3+\psi)}{\left(\bar{\lambda}_{p,\theta}/\sqrt{\xi_\theta}\right)^{1.5}} \quad \text{for } \bar{\lambda}_{p,\theta} > \bar{\lambda}_{p0,\theta} \tag{32}$$

The local buckling reduction factor ρ for slender outstand flange plates in austenitic stainless steel cross-sections is calculated by Eq. (33).

$$\rho = \frac{0.6}{\left(\bar{\lambda}_{p,\theta}/\sqrt{\xi_\theta}\right)^{0.6}} - \frac{0.075}{\left(\bar{\lambda}_{p,\theta}/\sqrt{\xi_\theta}\right)^{1.2}} \quad \text{for } \bar{\lambda}_{p,\theta} > \bar{\lambda}_{p0,\theta} \tag{33}$$

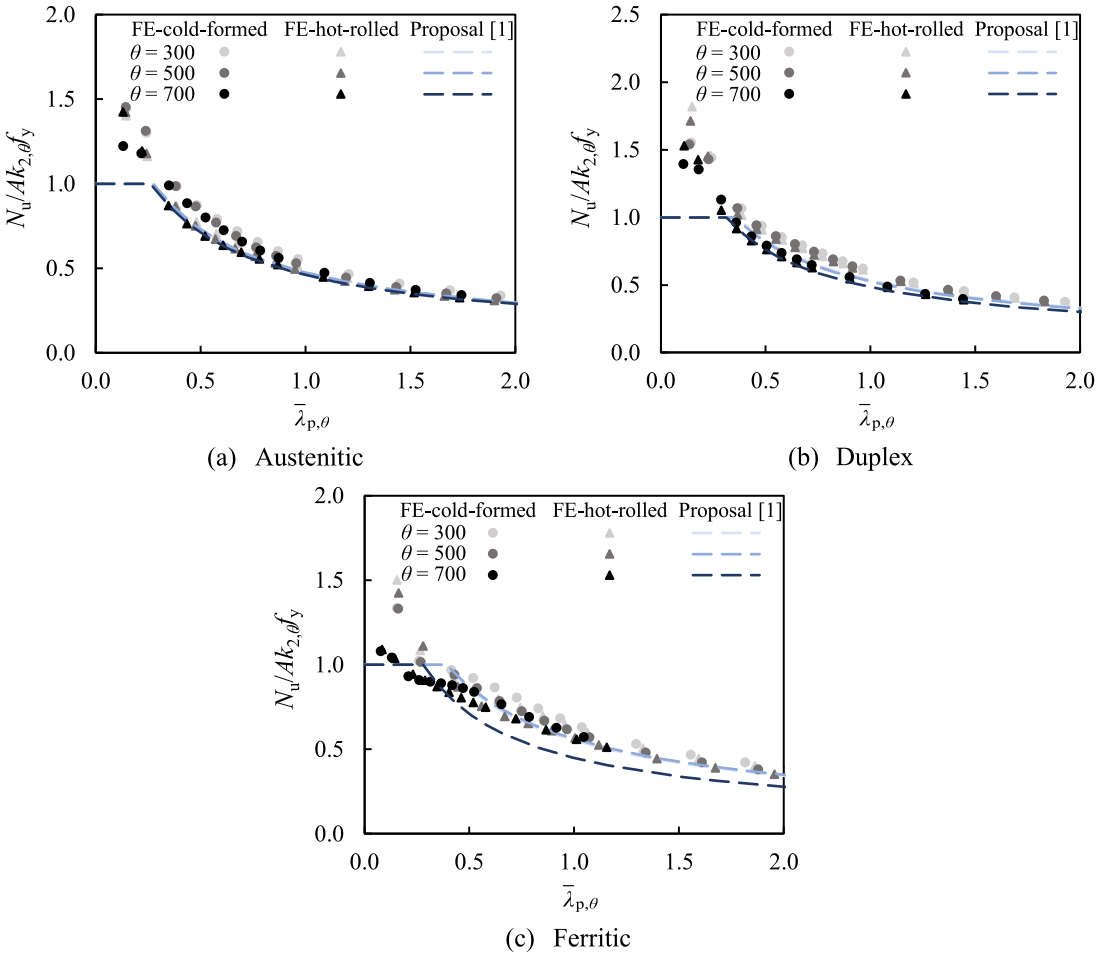

Fig. 10. Comparisons between the ultimate resistances determined using the design proposals in [9] against FE results for internal isolated stainless steel plates under compression at elevated temperatures.

On the other hand, the local buckling reduction factor ρ is determined by Eq. (34) for internal plate elements in duplex and ferritic stainless steel cross-sections

$$\rho = \frac{0.6}{\left(\overline{\lambda}_{p,\theta}/\sqrt{\xi_\theta}\right)^{0.75}} - \frac{0.015\,(3+\psi)}{\left(\overline{\lambda}_{p,\theta}/\sqrt{\xi_\theta}\right)^{1.5}} \quad \text{for } \overline{\lambda}_{p,\theta} > \overline{\lambda}_{p0,\theta} \tag{34}$$

and by Eq. (35) for outstand flange plates in duplex and ferritic stainless steel cross-sections.

$$\rho = \frac{0.67}{\left(\overline{\lambda}_{p,\theta}/\sqrt{\xi_\theta}\right)^{0.6}} - \frac{0.075}{\left(\overline{\lambda}_{p,\theta}/\sqrt{\xi_\theta}\right)^{1.2}} \quad \text{for } \overline{\lambda}_{p,\theta} > \overline{\lambda}_{p0,\theta} \tag{35}$$

As previously introduced, in Eqs. (32) and (34), $\psi = \sigma_2/\sigma_1$ is the ratio of the stresses at the two edges of the plate, where σ_1 is the maximum compressive stress (with compression positive) and σ_2 is the minimum compressive stress or maximum tensile stress σ_2 in accordance with the recommendations of EN 1993-1-5 [38]. Moreover, the threshold plate slendernesses $\overline{\lambda}_{p0,\theta}$ in Eqs. (32)–(35) should be correspondingly determined through Eqs. (23)–(26) for internal and outstand austenitic, duplex and ferritic stainless steel cross-section plate elements.

Fig. 10 presents comparisons between the ultimate resistances Nu determined using the design proposals in [9] against FE results for internal isolated hot-rolled stainless steel plates under compression at elevated temperatures. It can be seen from the figure that the effective width method used in this study provides accurate resistance predictions for isolated stainless steel plates at elevated temperatures.

4.2.2. Combined compression and bending

For stainless steel SHS and RHS subjected to combined compression and bending at elevated temperatures, the use of a linear interaction relationship between the cross-section axial compression resistance $N_{fi,t,Rd}$ and bending moment resistance $M_{fi,t,Rd}$ is recommended in the determination of the elevated temperature cross-section resistances in line with the proposals made in [9] for individual stainless steel plates. Thus, the cross-section strength can be assessed as given by Eq. (36).

$$\frac{N_{Ed}}{N_{fi,t,Rd}} + \frac{M_{Ed}}{M_{fi,t,Rd}} \leq 1.0 \tag{36}$$

Note that the cross-section axial compression resistances $N_{fi,t,Rd}$ and bending moment resistances $M_{fi,t,Rd}$ are independently determined with the classification of the cross-sections considering pure axial compression and pure bending loading cases, respectively. As shown in Fig. 9(c), if a cross-section is classified as 'non-slender' for both pure compression and pure bending conditions, the full cross-section area A and the plastic section modulus W_{pl} are used in the determination of the cross-section axial compression $N_{fi,t,Rd}$ and bending moment $M_{fi,t,Rd}$ resistances. On the other hand, if the cross-section is classified as 'slender' under pure compression but 'non-slender' under pure bending, the effective section area A_{eff} and the plastic section modulus W_{pl} should be used in the determination of the cross-section axial compression resistance $N_{fi,t,Rd}$ and bending moment resistance $M_{fi,t,Rd}$. Of course, if the cross-section is classified as 'slender' under both pure compression and pure bending loading cases, the effective area A_{eff} and effective

section modulus W_{eff} should be employed in the determination of $N_{\mathrm{fi,t,Rd}}$ and $M_{\mathrm{fi,t,Rd}}$, respectively.

4.2.3. Combined bending and shear

For stainless steel SHS and RHS subjected to combined bending and shear at elevated temperatures, the recommendations provided in the fire design standard EN 1993-1-2 [3], which directs designers to the room temperature design standard EN 1993-1-1 [49], for the consideration of the adverse effects from high shear forces have been adopted in this study. Thus, when the applied shear force V_{Ed} exceeds half the elevated temperature plastic shear capacity $V_{\mathrm{fi,t,Rd}}$, the designed bending moment capacity should be determined through the reduced elevated temperature material strengths at 2% total strain $f_{2,\theta,\mathrm{r}}$ as given by Eq. (37).

$$f_{2,\theta,\mathrm{r}} = \left(1-\rho_{\mathrm{v}}\right) k_{2,\theta} f_{\mathrm{y}}^{*} \tag{37}$$

In Eq. (37), the reduction factor ρ_{v} is determined by Eqs. (38)–(39) in line with EN 1993-1-1 [49].

$$\rho_{\mathrm{v}} = (2V/V_{\mathrm{fi,t,Rd}} - 1)^2 \text{ for } V > 0.5V_{\mathrm{fi,t,Rd}} \tag{38}$$

$$V_{\mathrm{fi,t,Rd}} = A_{\mathrm{v}} k_{2,\theta} f_{\mathrm{y}} \tag{39}$$

$$A_{\mathrm{v}} = \begin{cases} Ah/(b+h) \text{ for SHS and RHS under major axis} \\ \qquad \text{bending and shear} \\ Ab/(b+h) \text{ for RHS under minor axis bending and shear} \end{cases} \tag{40}$$

The recommended approach for the consideration of the influence of high shear effects on the ultimate resistances of stainless steel SHS and RHS at elevated temperatures is illustrated in Fig. 9(d), in which the shear-reduced bending capacity is calculated using the factor ($1-\rho_{\mathrm{v}}$) multiplied by the cross-section bending moment resistance. Similarly, the reduced cross-section axial compression resistances can also be calculated adopting the same approach, using the reduced elevated temperature material strengths at 2% total strain $f_{2,\theta,\mathrm{r}}$ for cross-sections subjected to combined axial compression and bending as well as high shear effects. It should be noted that in the determination of the elevated temperature plastic shear capacity $V_{\mathrm{fi,t,Rd}}$ of a cold-formed stainless steel SHS/RHS in Eq. (39), the 0.2% proof strengths of the flat regions f_{y} should be utilised. In the case of a hot-rolled stainless steel SHS/RHS, of course, the uniform 0.2% proof strength f_{y} across the cross-section is used to determine the elevated temperature plastic shear capacity $V_{\mathrm{fi,t,Rd}}$ of a cross-section through Eq. (39).

5. Assessment of the proposed fire design methods and EN 1993-1-2 for stainless steel SHS and RHS

This section presents the assessment of the accuracy of the cross-section fire design rules introduced in the previous section against the benchmark numerical data obtained from the developed FE models for cold-formed and hot-rolled stainless steel SHS and RHS at elevated temperatures. The proposed fire design rules are also compared against the design provisions of the European structural steel fire design standard EN 1993-1-2 [3] for the cross-section resistance predictions of cold-formed and hot-rolled stainless steel SHS and RHS at elevated temperatures.

5.1. Pure compression

5.1.1. Accuracy assessment

Figs. 11 and 12 show the comparisons between the ultimate resistance predictions obtained using the proposed fire design rules (see Section 4) $N_{\mathrm{u,prop}}$ and EN 1993-1-2 [3] (see Section 3) $N_{\mathrm{u,EC3}}$ against the benchmark FE ultimate resistance predictions $N_{\mathrm{u,FE}}$ for cold-formed and hot-rolled austenitic, duplex and ferritic stainless steel SHS under compression at elevated temperatures. In the figures, $\overline{\lambda}_{\mathrm{p,cs},\theta}$ is the elevated temperature cross-section slenderness determined through multiplying the room temperature cross-section slenderness $\overline{\lambda}_{\mathrm{p,cs}}$ by the elevated temperature strength-to-stiffness reduction ratio factor $\xi_{\theta} = \sqrt{k_{2,\theta}/k_{\mathrm{E},\theta}}$ (i.e. $\overline{\lambda}_{\mathrm{p,cs},\theta} = \overline{\lambda}_{\mathrm{p,cs}}\xi_{\theta} = \overline{\lambda}_{\mathrm{p,cs}}\sqrt{k_{2,\theta}/k_{E,\theta}}$). Note that the room temperature cross-section slenderness $\overline{\lambda}_{\mathrm{p,cs}}$ is calculated as $\overline{\lambda}_{\mathrm{p,cs}} = \sqrt{f_{\mathrm{y}}^{*}/\sigma_{\mathrm{cr,cs}}}$ in which $\sigma_{\mathrm{cr,cs}}$ is the elastic local buckling stress of the full cross-section. In this study, the elastic critical local buckling stresses of full stainless steel cross-sections $\sigma_{\mathrm{cr,cs}}$ were calculated through the formulae developed by Gardner et al. [50] for the predictions of the elastic critical buckling stresses of steel cross-sections; the calculations were carried out using the centreline dimensions in line with the recommendations of [50].

Table 9
Summary of mean, CoV, maximum and minimum values of the ratios of the resistance predictions obtained from FE modelling $N_{\mathrm{u,FE}}$ to those determined using the new proposals $N_{\mathrm{u,prop}}$ and the provisions of EN 1993-1-2 [3] $N_{\mathrm{u,EC3}}$ for all studied cold-formed and hot-rolled stainless steel SHS and RHS under compression at elevated temperatures.

Type	Grade	No.	$N_{\mathrm{u,FE}}/N_{\mathrm{u,prop}}$				$N_{\mathrm{u,FE}}/N_{\mathrm{u,EC3}}$			
			Mean	CoV	Max	Min	Mean	CoV	Max	Min
Cold-formed	A	180	1.05	0.028	1.13	0.99	1.12	0.086	1.30	0.87
	D	180	1.05	0.044	1.22	0.97	1.17	0.077	1.41	0.99
	F	180	1.11	0.079	1.32	0.95	1.06	0.118	1.45	0.88
Hot-rolled	A	200	1.01	0.118	1.46	0.90	1.06	0.127	1.46	0.78
	D	200	1.06	0.146	1.63	0.91	1.16	0.133	1.63	0.91
	F	200	1.04	0.085	1.23	0.85	1.05	0.118	1.44	0.79

As can be seen from Figs. 11 and 12, the proposed design rules lead to very accurate ultimate resistance predictions for cold-formed and hot-rolled stainless steel SHS at elevated temperatures. For hot-rolled austenitic and duplex stainless steel SHS at elevated temperatures, some of the ultimate resistance predictions obtained through the proposed design rules are slightly higher than those obtained through the finite element models as can be seen from Fig. 12(a) and (c). This was ascribed to the use of larger local geometric imperfection magnitudes in the FE models in this paper relative to those employed in [9] in the development of the effective width method for stainless steel plates at elevated temperatures adopted in this study. Nevertheless, as can be seen from Fig. 12(a) and (c), the overestimations which are only specific for this case are quite small (generally less than 5%) and Fig. 11 shows that the proposed fire design approach leads to very accurate ultimate resistance estimations for cold-formed stainless steel SHS at elevated temperatures, which are considerably more widely used in practice relative to hot-rolled stainless steel SHS.

Figs. 11 and 12 also show that the proposed design rules lead to a higher level of accuracy relative to EN 1993-1-2 [3] in the estimations of the ultimate compression resistances of cold-formed and hot-rolled stainless steel SHS at elevated temperatures. According to EN 1993-1-2 [3], (i) the elevated temperature strengths at 2% total strain $f_{2,\theta} = k_{2,\theta} f_{\mathrm{y}}^{*}$ are used as the reference material strengths to predict the cross-section resistances of Class 1, 2 and 3 cross-sections and (ii) the elevated temperature 0.2% proof strengths $f_{\mathrm{p0.2},\theta} = k_{\mathrm{p0.2},\theta} f_{\mathrm{y}}^{*}$ are used in the determination of the ultimate cross-section resistances of Class 4 cross-sections. This results in abrupt steps in the cross-section resistance predictions at the transitions from Class 3 to 4 cross-sections, as shown in Figs. 11 and 12. On the other hand, the proposed design rules recommend the consistent use of the elevated temperature material strengths at 2% total strain $f_{2,\theta} = k_{2,\theta} f_{\mathrm{y}}^{*}$ as the reference material strengths in the determination of the cross-section resistances for all cross-section classes, which leads to continuous capacity predictions changing with the cross-section slenderness as can be seen from Figs. 11 and 12. The accuracy of the proposed design rules is also extensively assessed for stainless steel RHS stub columns at elevated temperatures. Fig. 13 presents comparison of the ultimate resistance predictions obtained through the proposed design rules and EN 1993 1-2 for a

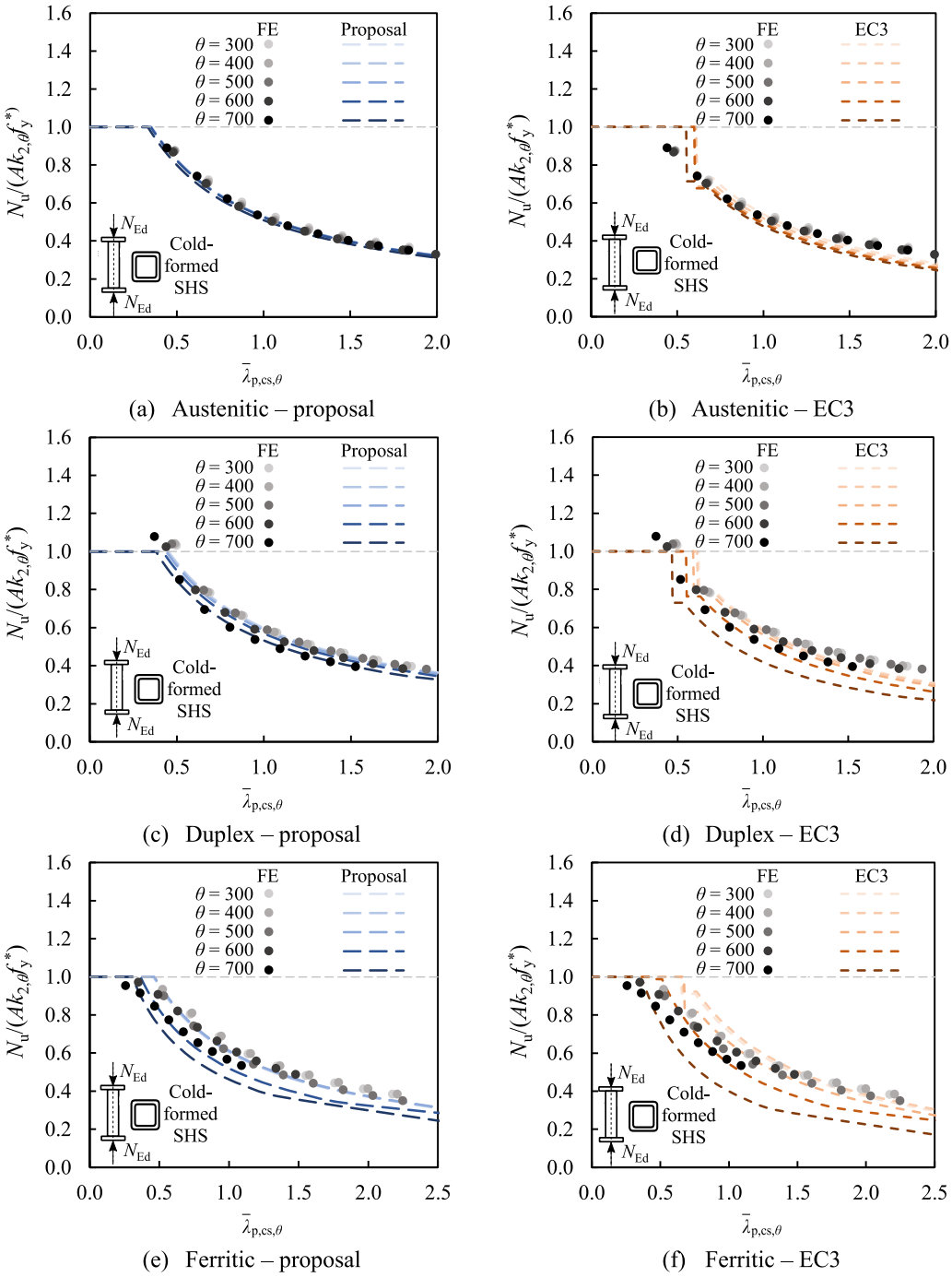

Fig. 11. Comparisons between the ultimate resistances determined through the proposed design method $N_{u,prop}$ and the provisions of EN 1993-1-2 $N_{u,EC3}$ against those obtained from FE modelling $N_{u,FE}$ for cold-formed stainless steel SHS under compression at elevated temperatures.

number of studied cold-formed and hot-rolled stainless steel RHS at elevated temperatures. As can be seen from Fig. 13, the proposed design rules also lead to a significantly improved level of accuracy in the ultimate resistance predictions of RHS subjected to pure axial compression at elevated temperatures relative to EN 1993-1-2 [3].

The assessment of the accuracy of the ultimate compression resistance predictions obtained using the proposed design rules $N_{u,prop}$ and the provisions of EN 1993-1-2 [3] $N_{u,EC3}$ against the benchmark FE ultimate resistance predictions $N_{u,FE}$ is presented in Fig. 14 for all the investigated 1140 cold-formed and hot-rolled SHS and RHS stub columns at elevated temperatures. A statistical evaluation of the accuracy of the proposed design rules and EN 1993-1-2 [3] is also provided in Table 9, where the mean, coefficient of variation (CoV), maximum and minimum values of the ratios of $N_{u,FE}/N_{u,prop}$ and $N_{u,FE}/N_{u,EC3}$ for all the studied stainless steel SHS and RHS stub columns are summarised. Note that since the thicknesses of the considered cold-formed cross-sections are limited to 6 mm (see Section 2.3), the numbers of the studied cases are different for cold-formed and hot-rolled stainless steel SHS/RHS at elevated temperatures. As can be seen from Fig. 14, relative to the design rules given in EN 1993-1-2 [3], the proposed design rules lead to considerably more accurate ultimate resistance predictions with a much lower scatter level for all the considered cold-formed and hot-rolled stainless steel SHS and RHS, taking into consideration a broad range of cross-section slendernesses

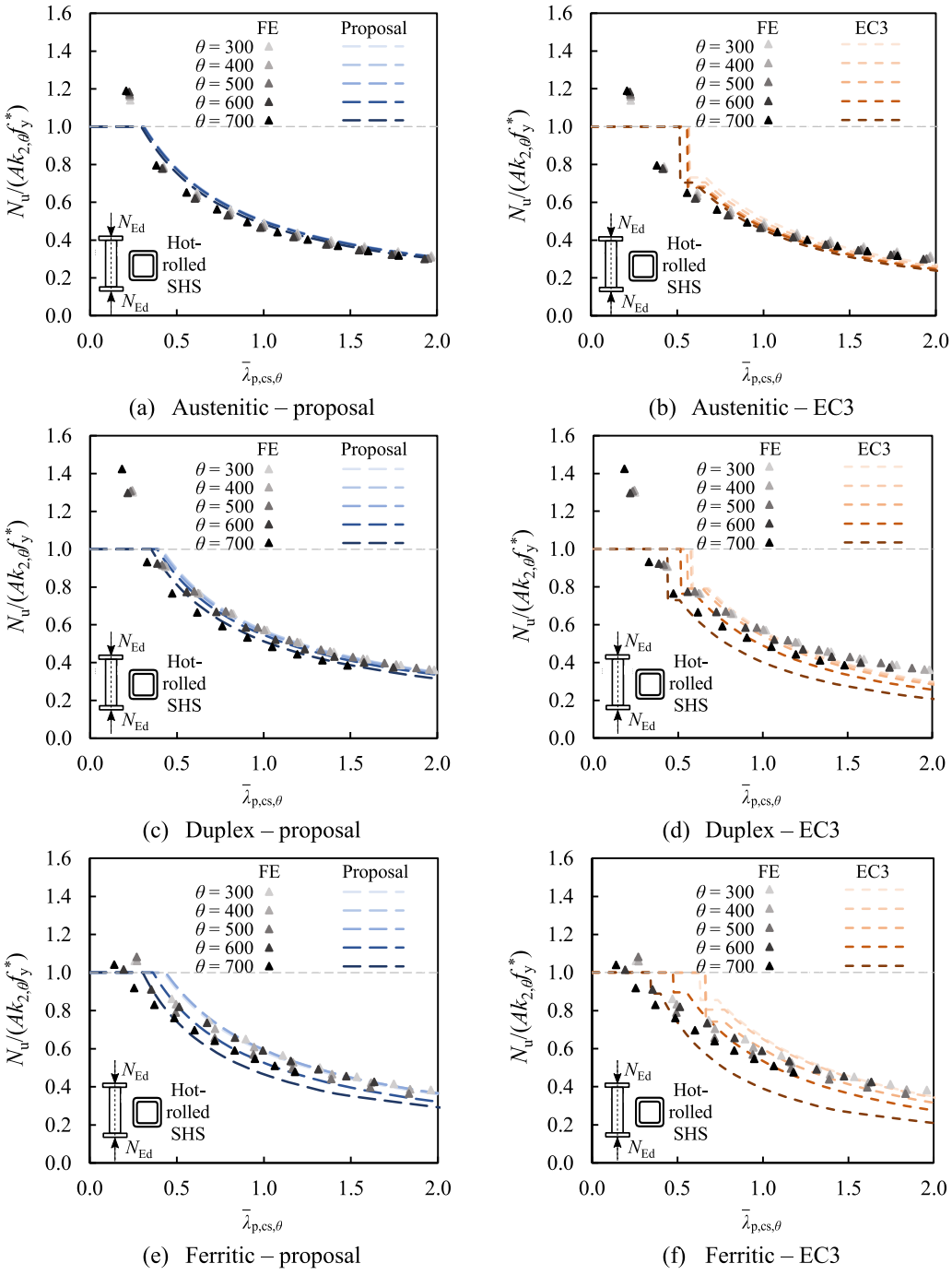

Fig. 12. Comparisons between the ultimate resistances determined through the proposed design method $N_{u,prop}$ and the provisions of EN 1993-1-2 $N_{u,EC3}$ against those obtained from FE modelling $N_{u,FE}$ for hot-rolled stainless steel SHS under compression at elevated temperatures.

and different elevated temperature levels. The higher accuracy of the proposed design rules relative to EN 1993-1-2 can also be observed in Table 9, where the mean values of the ratios $N_{u,FE}/N_{u,prop}$ are generally closer to 1.0 with lower CoV values relative to the corresponding mean and CoV values of $N_{u,FE}/N_{u,EC3}$. Note that as can be seen in Table 9, the hot-rolled duplex SHS and RHS group has larger CoV values of $N_{u,FE}/N_{u,prop}$ and $N_{u,FE}/N_{u,EC3}$; this is mainly due to the significant levels of strain hardening observed in a high number of stocky hot-rolled duplex stainless steel SHS and RHS as can be seen from Fig. 14.

The proposed cross-section fire design approach in this paper is based on the effective width method and does not consider the beneficial influence of the plate element interaction on the ultimate resistances of stainless steel cross-sections at elevated temperatures. This is an inherent feature of the effective width method where each plate is assessed individually, leading to the neglect of the beneficial effect from the plate element interaction within stainless steel cross-sections. The neglect of the plate element interaction within the proposed cross-section fire design method contributes to the scatter in the ratios

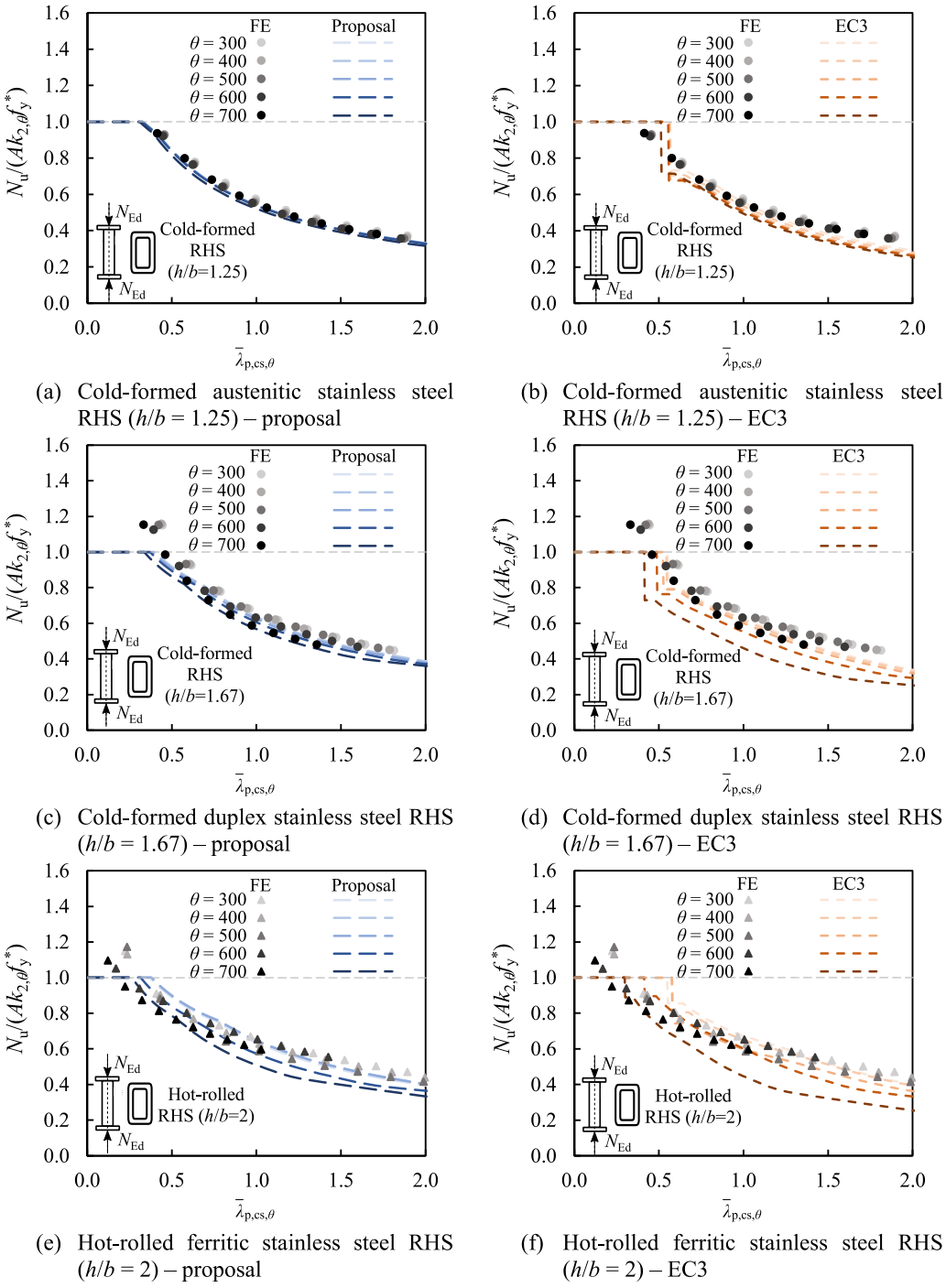

(a) Cold-formed austenitic stainless steel RHS (h/b = 1.25) – proposal

(b) Cold-formed austenitic stainless steel RHS (h/b = 1.25) – EC3

(c) Cold-formed duplex stainless steel RHS (h/b = 1.67) – proposal

(d) Cold-formed duplex stainless steel RHS (h/b = 1.67) – EC3

(e) Hot-rolled ferritic stainless steel RHS (h/b = 2) – proposal

(f) Hot-rolled ferritic stainless steel RHS (h/b = 2) – EC3

Fig. 13. Comparisons between the ultimate resistance predictions determined through the proposed design method $N_{u,prop}$ and the provisions of EN 1993-1-2 $N_{u,EC3}$, against those obtained from $N_{u,FE}$ for studied examples of stainless steel RHS under compression at elevated temperatures.

between the ultimate resistances obtained through the shell FE models and those determined through the proposed fire design method. Additionally, the proposed cross-section fire design approach adopts the elevated temperature material strength at 2% total strain in the determination of the cross-section resistances of stainless steel cross-sections at elevated temperatures. However, as shown the elevated temperature material stress–strain curves in Fig. 3, stainless steel can exhibit strain hardening at elevated temperatures and attain the elevated temperature material strengths that are higher than the elevated temperature material strengths at 2% strain. This strain hardening observed in stocky stainless steel cross-sections at elevated temperatures is not considered in the proposed cross-section fire design approach. The Continuous Strength Method [51] is a deformation-based cross-section design approach and considers the beneficial influence of both plate element interaction and strain hardening on the ultimate resistances of stainless steel cross-sections. Future research will focus on the extension of the Continuous Strength Method to the cross-section fire design of stainless steel cross-sections whereby less scatter in the ultimate

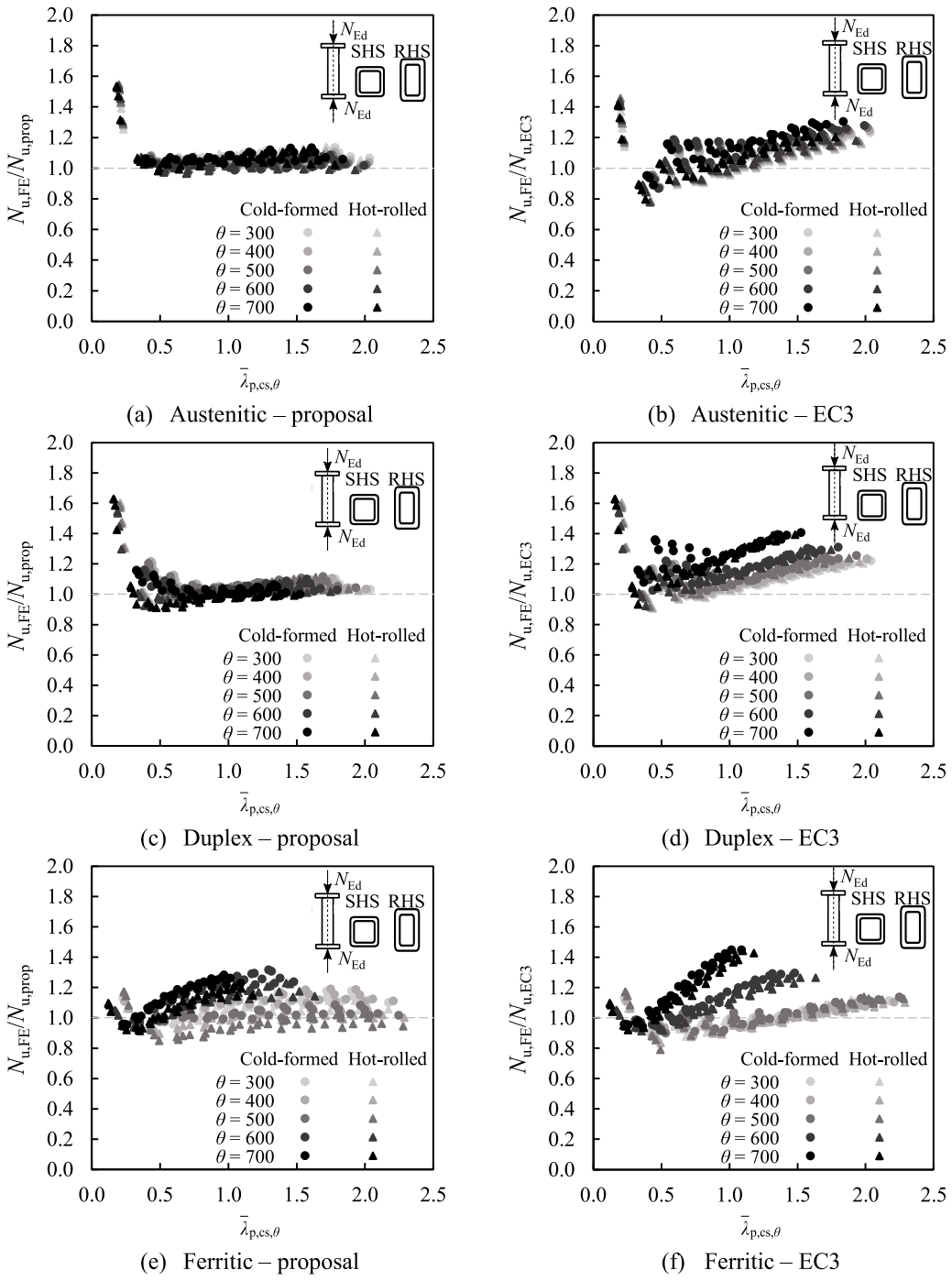

Fig. 14. Assessment of the accuracy of the ultimate cross-section resistance predictions determined through the proposed design method $N_{u,prop}$ and the provisions of EN 1993-1-2 $N_{u,EC3}$ against those obtained from FE modelling $N_{u,FE}$ for cold-formed and hot-rolled stainless steel SHS and RHS under compression at elevated temperatures.

resistance predictions of stainless steel cross-sections at elevated temperatures could be attained. It should however be emphasised that this study adopts the effective width concept considering that it is the primary cross-section design concept used in different parts of Eurocode 3.

The relatively lower accuracy of the European structural steel fire design standard EN 1993-1-2 [3] for stainless steel SHS and RHS under pure axial compression at elevated temperatures, which is also observed in the upcoming subsections for different loading cases can be primarily attributed to its adoption of the room temperature cross-section design rules provided in EN 1993-1-4 [5] with the elevated temperature material properties of stainless steel for the fire design of stainless steel cross-sections. Since the elevated temperature material response of stainless steel can be significantly different than the room temperature material response with differential erosion rates of material strengths and stiffnesses, the use of the room temperature local buckling design rules can lead to inaccurate estimations of the behaviour in the fire design of stainless steel cross-sections as observed in this study. Recognising this, in the new proposed design rules, the use of the elevated temperature plate slendernesses $\overline{\lambda}_{p,\theta}$ which feature the elevated temperature strength-to-stiffness reduction ratio factor $\xi_\theta = \sqrt{k_{2,\theta}/k_{E,\theta}}$ is recommended (i) in the cross-section classification and

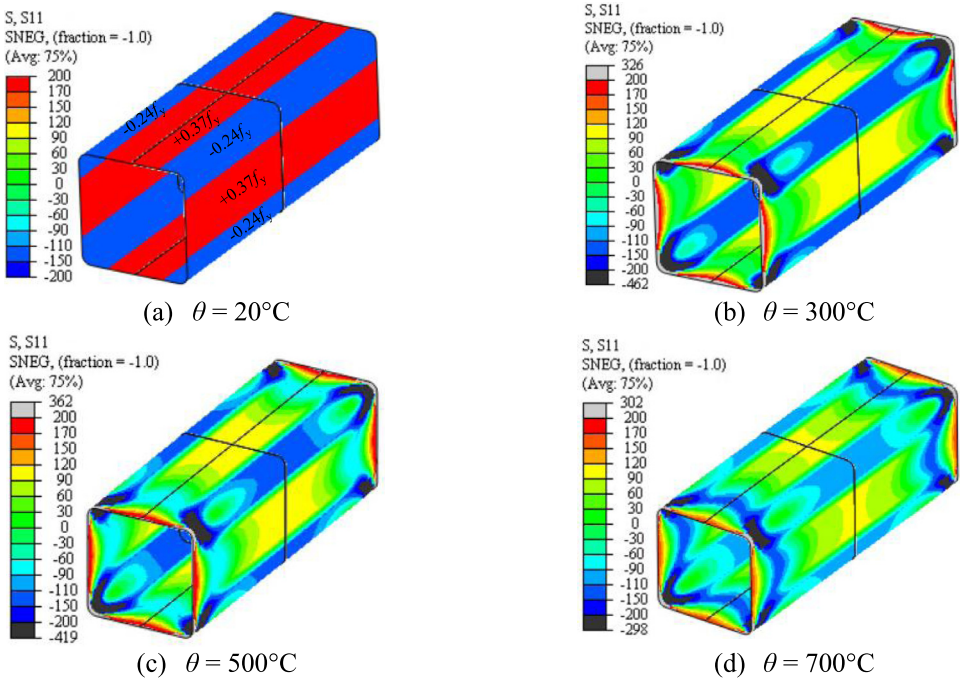

Fig. 15. Membrane residual stresses within the shell FE models of cold-formed austenitic stainless steel SHS stub columns ($\overline{\lambda}_{p,H,c} = 0.4$) with increasing elevated temperature levels (stresses in MPa).

(ii) in the determination of the local buckling reduction factors ρ for stainless steel cross-sections at elevated temperatures. The use of the elevated temperature plate slenderness $\overline{\lambda}_{p,\theta}$ enables the consideration of the different deterioration levels of material strength and stiffness of stainless steel at elevated temperatures, thereby leading to an accurate assessment of the behaviour of stainless steel cross-sections at elevated temperatures.

As indicated in Section 2.1.3, due to its negligible influence on the cross-section resistances of stainless steel SHS/RHS at elevated temperatures, residual stresses were not included in the FE models of stainless steel SHS/RHS in this study. The influence of the membrane residual stresses on the cross-section resistances of cold-formed stainless steel SHS/RHS is assessed herein, comparing the ultimate cross-section resistances obtained from the FE models with and without membrane residual stresses. In the FE models with residual stresses, the membrane residual stress pattern proposed by [14] for cold-formed stainless steel SHS/RHS was employed, where the tensile residual stress within the flat parts is taken as $0.37f_y$ and the compressive residual stress at the corner regions is taken as $0.24f_y$ as shown in Fig. 15(a). Fig. 15 presents the membrane residual stresses within the shell FE models of cold-formed austenitic stainless steel SHS stub columns ($\overline{\lambda}_{p,H,c} = 0.4$) at room temperature, 300 °C, 500 °C and 700 °C. It can be seen that with the development of thermal strains, the residual stresses dissipate with increasing temperatures. Fig. 16 shows comparisons between the ultimate compressive resistances obtained from the FE models with and without membrane residual stresses for cold-formed austenitic stainless steel SHS at 300 °C, 500 °C and 700 °C. It can be seen from Fig. 16 that the membrane residual stresses within stainless steel SHS/RHS have very small influence on the cross-section resistances of stainless steel SHS/RHS at elevated temperatures.

5.1.2. Reliability assessment

In this study, the reliability of the proposed design rules and the design provisions of EN 1993-1-2 [3] is assessed through the three reliability criteria put forward by Kruppa [52], which were also used in [7,53]. Criterion 1 of Kruppa [52] requires that none of the resistance predictions obtained using a design method should be higher than the benchmark FE results by more than 15% (i.e. max $[(N_{u,method} - N_{u,FE})/N_{u,FE}] \leq 15\%$), Criterion 2 of [52] states that less than 20% of the design predictions should be on the unsafe side (i.e. $\text{num}(N_{u,method} > N_{u,FE})/\text{num}(N_{u,FE}) \leq 20\%$) and Criterion 3 of [52] requires that the design predictions should be safe-sided on average (i.e. $\overline{X}[(N_{u,method} - N_{u,FE})/N_{u,FE}] < 0\%$). The reliability assessment of the proposed design rules and EN 1993-1-2 is summarised in Table 10 for all the studied cold-formed and hot-rolled stainless steel SHS and RHS stub columns in accordance with the three reliability criteria of Kruppa [52]. In Table 10, (i) Criterion 1 refers to the percentage of unsafe resistance predictions which exceed the benchmark FE results by more than 15%, (ii) Criterion 2 refers to the percentage of unsafe resistance predictions and (iii) Criterion 3 refers to the average of percentage differences between the resistance predictions obtained using a design method and the benchmark FE models. As can be seen from Table 10, for all the considered cold-formed stainless steel SHS and RHS, the proposed fire design rules satisfy all the three criteria of Kruppa [52], while EN 1993-1-2 [3] slightly violates Criterion 1 (as highlighted with '*') for cold-formed austenitic stainless steel SHS and RHS. EN 1993-1-2 [3] also violates Criterion 2 for cold-formed ferritic stainless steel SHS and RHS since the percentage of the unsafe predictions is equal to 40% which is higher than the limit value of 20%.

For hot-rolled stainless steel SHS and RHS at elevated temperatures, both the proposed design rules and EN 1993-1-2 violate the reliability criteria for some groups. However, in the case of the new proposed design rules, these violations simply stem from the ultimate resistance predictions that are only slightly higher than the benchmark FE ultimate resistances for hot-rolled stainless steel SHS and RHS at elevated temperatures as can be seen from Table 9 and Fig. 14. As previously mentioned, the slightly higher ultimate resistance predictions of the proposed design rules for some hot-rolled stainless steel SHS and RHS primarily result from the use of larger local geometric imperfection magnitudes in the finite element models within this study relative to those used in the development of the effective width method of [9] which was adopted in the proposed design rules herein. In the present

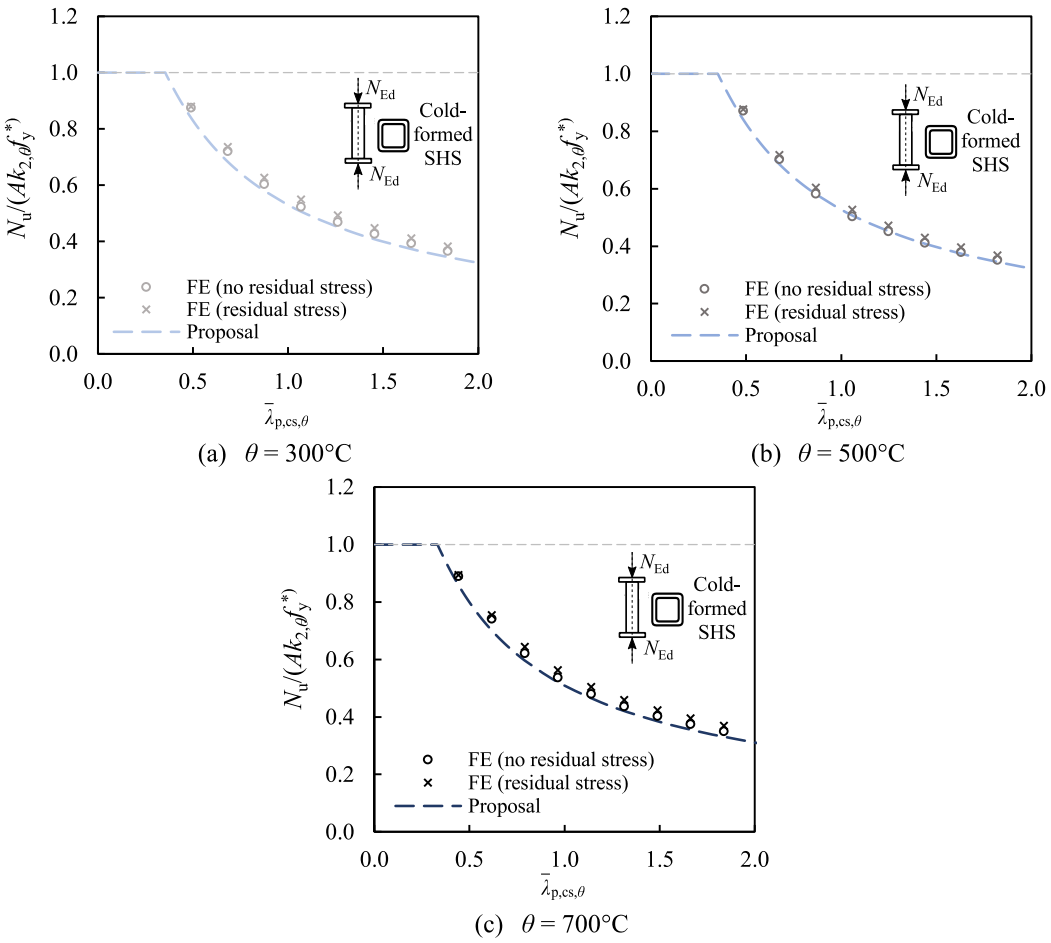

Fig. 16. Influence of residual stresses on cold-formed austenitic stainless steel SHS for different elevated temperature levels.

study, the local imperfection amplitudes incorporated into the benchmark FE models were taken as 80% of 1/100 of the largest flat plate widths h/100 for SHS and RHS stub columns, which were greater than the local geometric imperfection magnitudes taken equal to 1/200 of the plate widths in [9] for internal isolated plates. Table 11 presents the accuracy and reliability assessment of the proposed design rules against the numerical results obtained from the shell FE models of SHS/RHS with local geometric imperfection magnitudes taken equal to 1/200 of flat widths of the critical plates for all the studied SHS and RHS stub columns, using the local geometric imperfection values adopted in [9] for isolated internal plates. It can be seen from Table 11 that the proposed design rules are generally very accurate and safe when the local geometric imperfection magnitudes adopted in [9] are used, and only very slightly violate Criterion 2 of Kruppa [52] for hot-rolled austenitic and ferritic cross-sections, which can be deemed to be within an acceptable range in accordance with [54,55]. Moreover, for cold-formed stainless steel SHS and RHS at elevated temperatures which are considerably more widely used relative to hot-rolled stainless steel SHS and RHS, very accurate and safe axial compression resistance predictions are obtained through the proposed design rules for all the cases as illustrated in Tables 9 and 10 with the satisfaction of all the three reliability criteria of Kruppa [52].

Finally, it is worth noting that as can be seen from Figs. 11, 12 and 14, relative to hot-rolled stainless steel SHS/RHS, slightly higher normalised ultimate strengths can be observed for cold-formed stainless steel SHS/RHS. This can be ascribed to the differences in the material strengths within cold-formed and hot-rolled stainless steel cross-sections. Typically, cold-formed stainless steel cross-sections possess higher material strengths which lead to more nonlinear stress distributions across their plate elements at collapse after the occurrence of elastic local buckling, resulting in more enhanced post-buckling strengths relative to those for hot-rolled stainless steel cross-sections in accordance with the von Karman [56] and Winter [57] plate failure concepts.

5.2. Pure bending

5.2.1. Accuracy assessment

Figs. 17 and 18 show the comparisons between the ultimate resistance predictions obtained using the design rules proposed in this paper and EN 1993-1-2 [3] against those obtained from the shell FE models for the studied cold-formed and hot-rolled stainless steel SHS under bending. Similar to the observations made for SHS and RHS under pure compression at elevated temperatures, relative to EN 1993-1-2 [3], the proposed design rules also lead to a considerably improved level of accuracy for stainless steel SHS subjected to bending at elevated temperatures. Comparisons between the ultimate resistances determined through the proposed design rules and EN 1993-1-2 against those obtained from the shell FE models are also shown for a number of studied stainless steel RHS beams subjected to pure major or minor axis bending in Fig. 19. As can be seen from the figure, the proposed design rules also provide more accurate resistance predictions for stainless steel RHS under pure major or minor axis at elevated temperatures relative to EN 1993-1-2 [3].

The assessment of the accuracy of the ultimate bending resistance predictions obtained using the proposed design rules $M_{u,prop}$ and EN 1993-1-2 [3] $M_{u,EC3}$ against those obtained from the shell FE models $M_{u,FE}$ are shown in Fig. 20 for all the investigated 1995 cold-formed

Table 10
Reliability assessment of the new proposals and the provisions of EN 1993-1-2 [3] for all studied cold-formed and hot-rolled stainless steel SHS and RHS under compression at elevated temperatures.

Type	Grade	New proposals			EN 1993-1-2		
		Criterion 1 (%)	Criterion 2 (%)	Criterion 3 (%)	Criterion 1 (%)	Criterion 2 (%)	Criterion 3 (%)
Cold-formed	A	0.00	3.33	−4.88	0.56*	12.22	−10.25
	D	0.00	5.56	−4.97	0.00	1.67	−13.76
	F	0.00	12.22	−9.09	0.00	40.00*	−4.38
Hot-rolled	A	0.00	65.50*	0.35*	5.00*	33.50*	−4.07
	D	0.00	33.00*	−4.28	0.00	11.50	−12.07
	F	1.00*	39.50*	−2.75	2.00*	41.50*	−3.47

*Violated criterion.

Table 11
Summary of accuracy and reliability assessment of the new design proposals against the numerical results obtained from the shell FE models including local imperfection amplitudes equal to 1/200 of the flat widths of the critical plates for all studied cold-formed and hot-rolled stainless steel SHS and RHS under compression at elevated temperatures.

Type	Grade	$N_{u,FE}/N_{u,prop}$				Reliability assessment		
		Mean	CoV	Max	Min	Criterion 1 (%)	Criterion 2 (%)	Criterion 3 (%)
Cold-formed	A	1.09	0.029	1.16	1.01	0.00	0.00	−7.82
	D	1.09	0.049	1.27	1.01	0.00	0.00	−7.96
	F	1.14	0.084	1.35	0.97	0.00	2.78	−12.03
Hot-rolled	A	1.06	0.129	1.55	0.93	0.00	31.00*	−4.36
	D	1.12	0.166	1.78	0.96	0.00	6.50	−8.55
	F	1.08	0.089	1.28	0.90	0.00	24.50*	−6.99

*Violated criterion.

Table 12
Summary of mean, CoV, maximum and minimum values of the ratios of the resistance predictions obtained from FE modelling $M_{u,FE}$ to those determined using the new proposal $M_{u,prop}$ and the provisions of EN 1993-1-2 [3] $M_{u,EC3}$ for all studied cold-formed and hot-rolled stainless steel SHS and RHS under major or minor axis bending at elevated temperatures.

Type	Grade	No.	$M_{u,FE}/M_{u,prop}$				$M_{u,FE}/M_{u,EC3}$			
			Mean	CoV	Max	Min	Mean	CoV	Max	Min
Cold-formed	A	315	1.20	0.039	1.32	1.07	1.29	0.142	1.57	0.87
	D	315	1.23	0.053	1.42	1.09	1.35	0.113	1.70	1.01
	F	315	1.23	0.088	1.45	0.96	1.18	0.122	1.59	0.89
Hot-rolled	A	350	1.11	0.103	1.75	0.96	1.18	0.147	1.75	0.74
	D	350	1.15	0.090	1.66	0.94	1.26	0.130	1.66	0.82
	F	350	1.12	0.086	1.34	0.91	1.14	0.131	1.57	0.76

and hot-rolled stainless steel SHS and RHS subjected to pure bending at elevated temperatures (see Section 2.3 for the wide range of considered parameters). Fig. 20 shows that relative to EN 1993-1-2 [3], the proposed design rules furnish significantly more accurate and consistent ultimate bending resistance predictions for all the considered SHS and RHS under pure bending at elevated temperatures. Similar observations with respect to the significantly higher level of accuracy of the proposed design rules relative to EN 1993-1-2 [3] can also be made from the statistical evaluations in Table 12 for all the considered 1995 stainless steel cold-formed and hot-rolled SHS and RHS at elevated temperatures. As can be seen in Table 10, the mean values of the ratios between the ultimate resistances obtained from the shell FE and those determined through the proposed design rules $M_{u,FE}/M_{u,prop}$ are generally closer to 1.0 with lower CoV values relative to the corresponding values calculated for the ratios between the ultimate resistances determined through the shell FE models and those obtained from EN 1993-1-2 [3] $M_{u,FE}/M_{u,EC3}$. As can be seen in Fig. 20 and Table 12, in some cases, EN 1993-1-2 [3] provides unsafe ultimate bending resistance predictions for stainless steel SHS and RHS at elevated temperatures. By contrast, the proposed design rules lead to safe and accurate ultimate bending moment resistance predictions for stainless steel SHS and RHS at elevated temperatures in all the considered broad range of cases.

5.2.2. Reliability assessment

The reliability assessment of the proposed design rules and EN 1993-1-2 [3] on the basis of the three reliability criteria of Kruppa [52] is summarised in Table 13 for all the studied 1995 stainless steel cold-formed and hot-rolled SHS and RHS under bending at elevated temperatures. It can be seen that the proposed design rules satisfy all the three reliability criteria of Kruppa [52] for all the studied cases, while EN 1993-1-2 [3] violates Criterion 1 for the stainless steel hot-rolled SHS and RHS subjected to bending at elevated temperatures owing to the most unsafe bending resistance predictions exceeding the corresponding benchmark FE results by more than 15%. This demonstrates that the proposed design rules lead to more reliable ultimate bending resistance predictions for cold-formed and hot-rolled stainless-steel SHS and RHS under bending at elevated temperatures relative to EN 1993-1-2 [3].

5.3. Combined compression and bending

5.3.1. Accuracy assessment

The proposed fire design rules for SHS and RHS subjected to combined axial compression and bending described in Section 4.2 recommend the adoption of a linear interaction relationship between the pure compression and pure bending resistances as given by Eq. (36) and shown in Fig. 9(c). In accordance with the new fire design proposal of this paper, Fig. 21 shows the normalised ultimate strengths of the studied cold-formed and hot-rolled stainless steel SHS stub beam–columns. In Fig. 21, (i) the ultimate compression resistances obtained from the FE models $N_{u,FE}$ are normalised by the cross-section axial compression resistances calculated using the proposed design rules $N_{fi,t,Rd,prop}$(i.e. $N_{u,FE}/N_{fi,t,Rd,prop}$) and (ii) the bending moment resistances obtained from the FE models $M_{u,FE}$ are normalised by the cross-section bending moment resistances determined through the proposed design rules $M_{fi,t,Rd,prop}$ (i.e. $M_{u,FE}/M_{fi,t,Rd,prop}$). As can be seen in Fig. 21, the recommended linear interaction expression given by Eq. (36) leads to safe and generally accurate ultimate resistance predictions for stainless steel SHS under combined compression and bending at elevated temperatures. Similar observations can also be made in Fig. 22 for stainless steel RHS subjected to axial compression plus

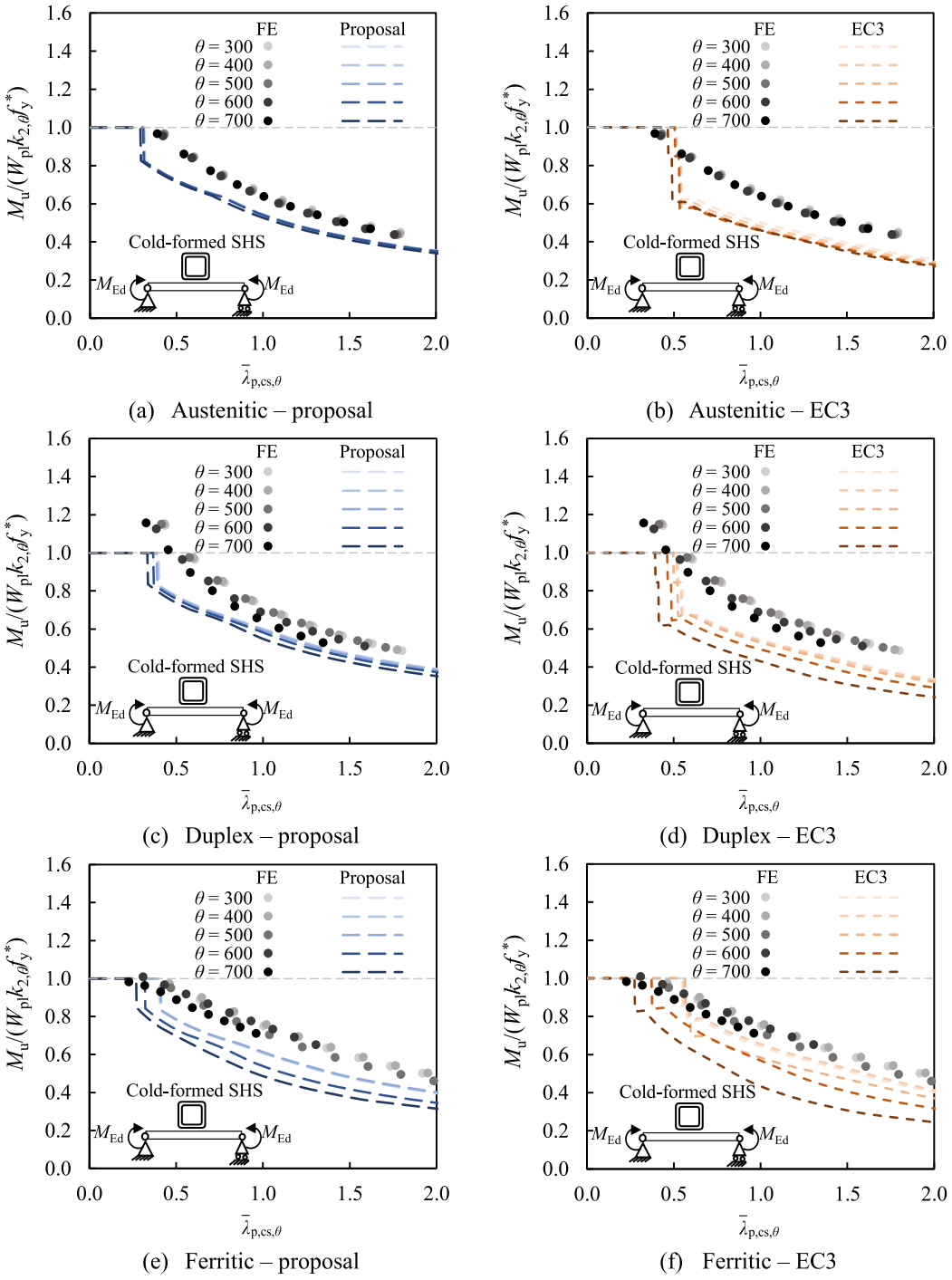

Fig. 17. Comparisons between the ultimate resistances determined through the proposed design method $M_{u,prop}$ and the provisions of EN 1993-1-2 $M_{u,EC3}$ against those obtained from FE modelling $M_{u,FE}$ for cold-formed stainless steel SHS under bending at elevated temperatures.

Table 13
Reliability assessment of the new proposals and the provisions of EN 1993-1-2 [3] for all studied cold-formed and hot-rolled stainless steel SHS and RHS under bending at elevated temperatures.

Type	Grade	Proposal			EN 1993-1-2		
		Criterion 1 (%)	Criterion 2 (%)	Criterion 3 (%)	Criterion 1 (%)	Criterion 2 (%)	Criterion 3 (%)
Cold-formed	A	0.00	0.00	−16.56	0.00	12.70	−20.70
	D	0.00	0.00	−18.47	0.00	0.00	−25.07
	F	0.00	6.67	−17.70	0.00	14.92	−14.05
Hot-rolled	A	0.00	4.00	−9.45	7.14*	14.00	−13.27
	D	0.00	3.14	−12.64	1.43*	10.57	−18.85
	F	0.00	11.71	−9.70	3.43*	18.57	−10.55

*Violated criterion.

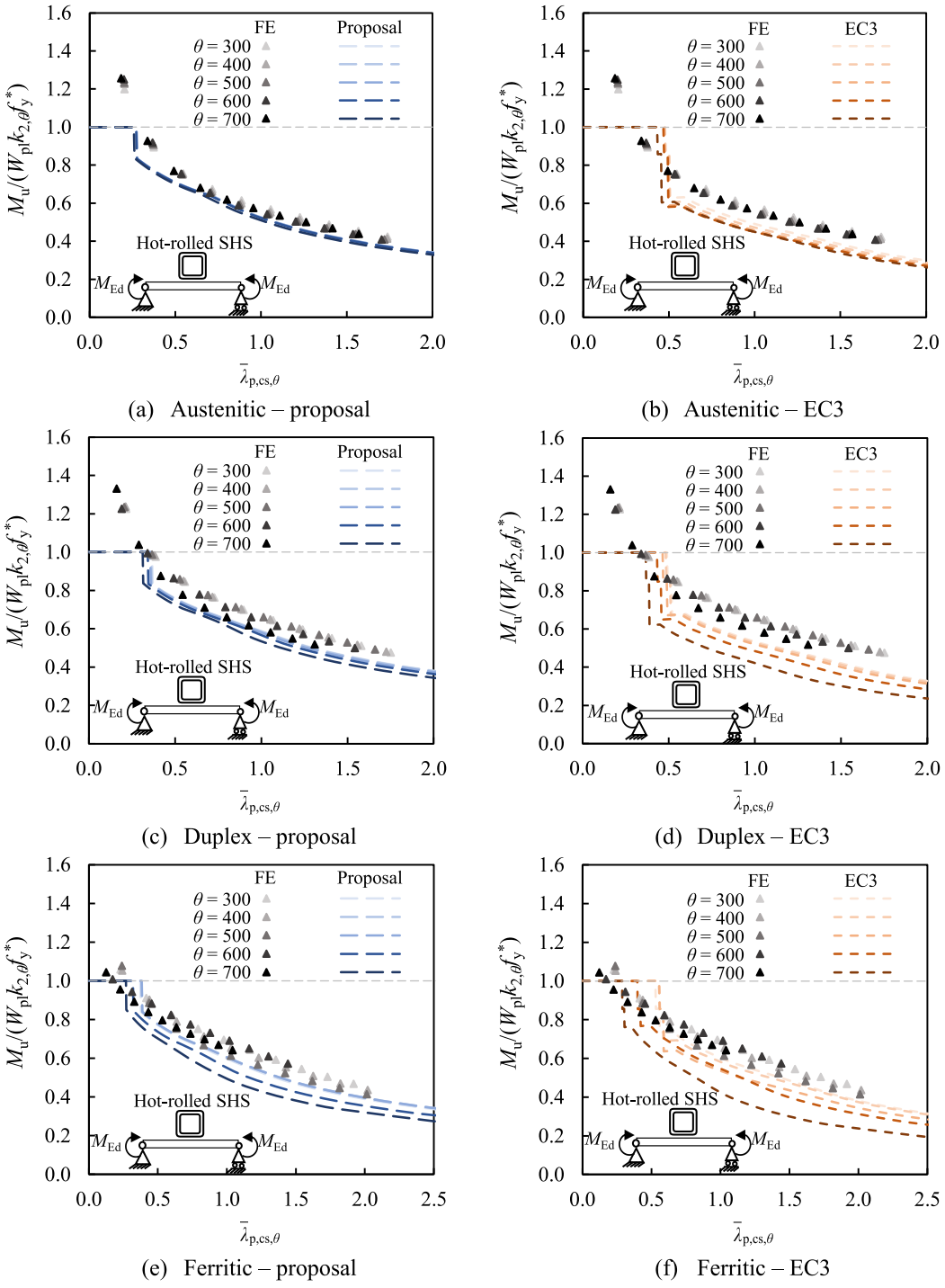

Fig. 18. Comparisons between the ultimate bending moment resistances determined through the proposed design method $M_{u,prop}$ and the provisions of EN 1993-1-2 $M_{u,EC3}$ against those obtained from FE modelling $M_{u,FE}$ for hot-rolled stainless steel SHS under bending at elevated temperatures.

bending at elevated temperatures, which shows the comparisons between the normalised FE resistance predictions (i.e. $N_{u,FE}/N_{fi,t,Rd,prop}$, $M_{u,FE}/M_{fi,t,Rd,prop}$) and the recommended linear interaction expression for a number of stainless steel RHS stub beam–columns under axial compression plus major or minor axis bending.

Fig. 23 shows the comparisons of the ultimate axial compression resistance predictions obtained using the new proposals $N_{u,prop}$ and EN 1993-1-2 $N_{u,EC3}$ against those from the benchmark FE models $N_{u,FE}$ for all the studied 6825 stainless steel cold-formed and hot-rolled SHS and RHS stub beam–columns subjected to combined axial compression and major or minor axis bending at elevated temperatures. In Fig. 23, comparisons are made for different radial angles ϕ for all the considered stainless steel SHS and RHS stub beam–columns. As described in Fig. 8, the parameter radial angle ϕ ranging between 0° and 90° represents the relative intensities of the applied compression and bending, where ϕ = 0° and ϕ = 90° correspond to pure bending and pure axial compression, respectively. As can be seen from Fig. 23, for different intensities of axial compression and bending, the new proposals lead to more accurate ultimate resistance predictions with a lower scatter level relative to EN 1993-1-2 [3] for the considered broad range of cold-formed and hot-rolled stainless steel SHS and RHS stub beam–columns

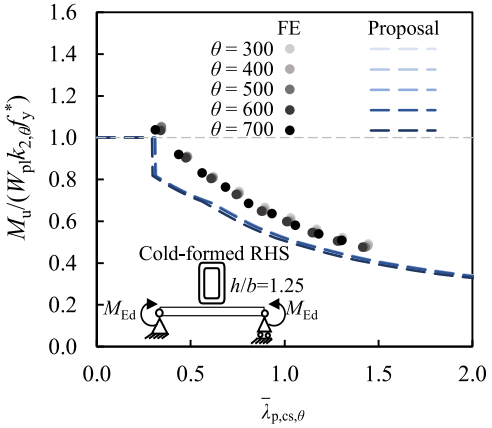

(a) Cold-formed austenitic stainless steel RHS (h/b = 1.25) under major axis bending – proposal

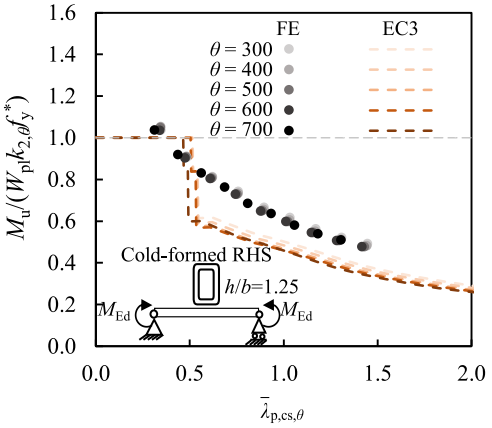

(b) Cold-formed austenitic stainless steel RHS (h/b = 1.25) under major axis bending – EC3

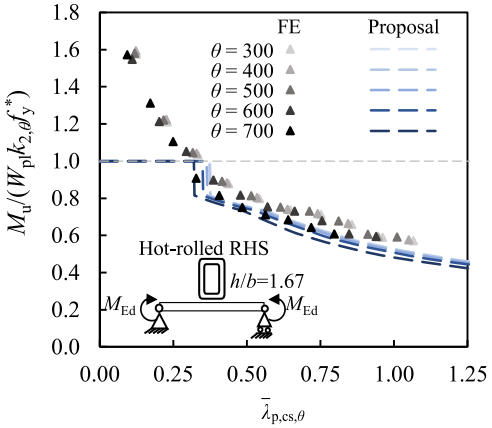

(c) Hot-rolled duplex stainless steel RHS (h/b = 1.67) under major axis bending – proposal

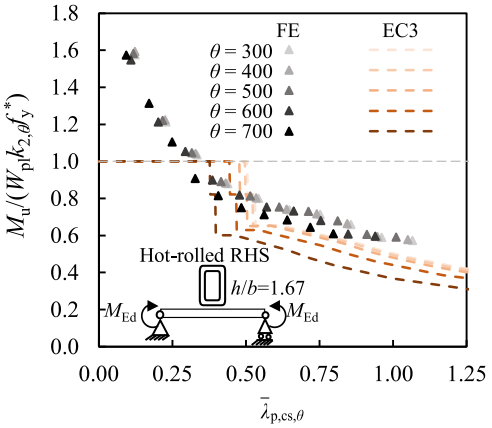

(d) Hot-rolled duplex stainless steel RHS (h/b = 1.67) under major axis bending – EC3

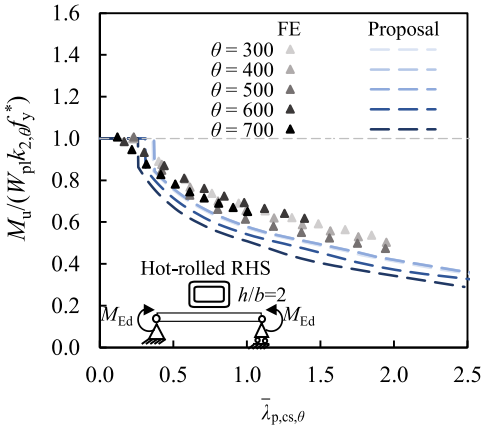

(e) Hot-rolled ferritic stainless steel RHS (h/b = 2) under minor axis bending – proposal

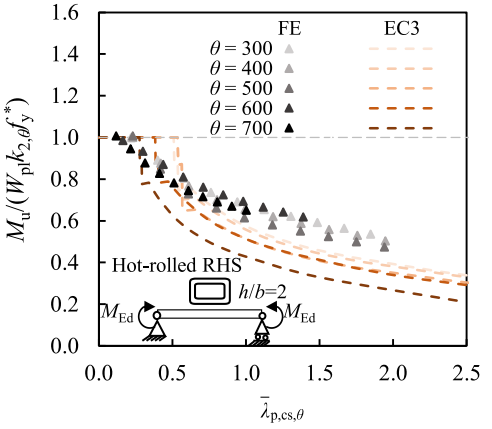

(f) Hot-rolled ferritic stainless steel RHS (h/b = 2) under minor axis bending – EC3

Fig. 19. Comparisons between the bending moment resistances determined through the proposed design method $M_{u,prop}$ and the provisions of EN 1993-1-2 $M_{u,EC3}$ against those obtained from FE modelling $M_{u,FE}$ for studied examples of stainless steel RHS under bending at elevated temperatures.

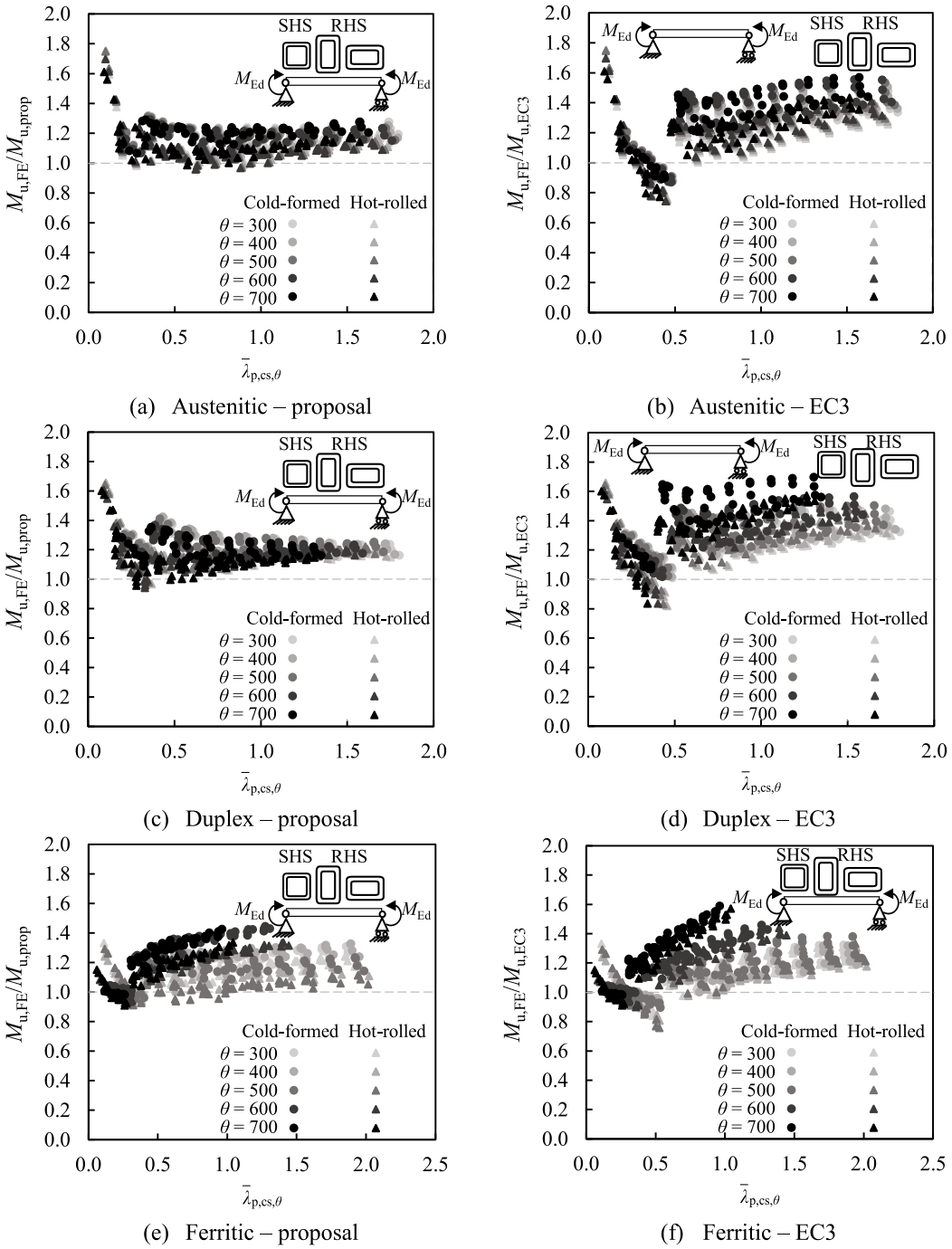

Fig. 20. Assessment of the accuracy of the ultimate cross-section bending moment resistances determined through the proposed design method $M_{u,prop}$ and the provisions given in EN 1993-1-2 $M_{u,EC3}$ against those obtained from FE modelling $M_{u,FE}$ for cold-formed and hot-rolled stainless steel SHS and RHS under major or minor axis bending at elevated temperatures.

under combined axial compression and bending at elevated temperatures. Fig. 23 also shows that a considerable number of EN 1993-1-2 [3] predictions are on the unsafe side. Similar observations can also be made from Table 14, which summarises a statistical assessment of the accuracy of the new fire design proposals (with $N_{u,FE}/N_{u,prop}$) and EN 1993-1-2 [3] (with $N_{u,FE}/N_{u,EC3}$) for all the studied SHS and RHS stub beam–columns at elevated temperatures. It can be seen from Table 14 that (i) the new proposals lead to significantly lower CoV values for $N_{u,FE}/N_{u,prop}$ relative to those for $N_{u,FE}/N_{u,EC3}$ and (ii) the minimum values of $N_{u,FE}/N_{u,prop}$ are significantly closer to 1.0 relative to the minimum values of $N_{u,FE}/N_{u,EC3}$ which highlight the considerably higher level of safety of the proposed design rules. As can be seen in Table 14, the minimum $N_{u,FE}/N_{u,EC3}$ values are quite smaller than 1.0, signifying the high level of unsafety of EN 1993-1-2 [3] for some stainless SHS and RHS stub beam–columns at elevated temperatures.

5.3.2. Reliability assessment

Table 15 presents the reliability assessment of the proposed design rules and EN 1993-1-2 [3] using the three reliability criteria of Kruppa [52] for all the studied cold-formed and hot-rolled stainless

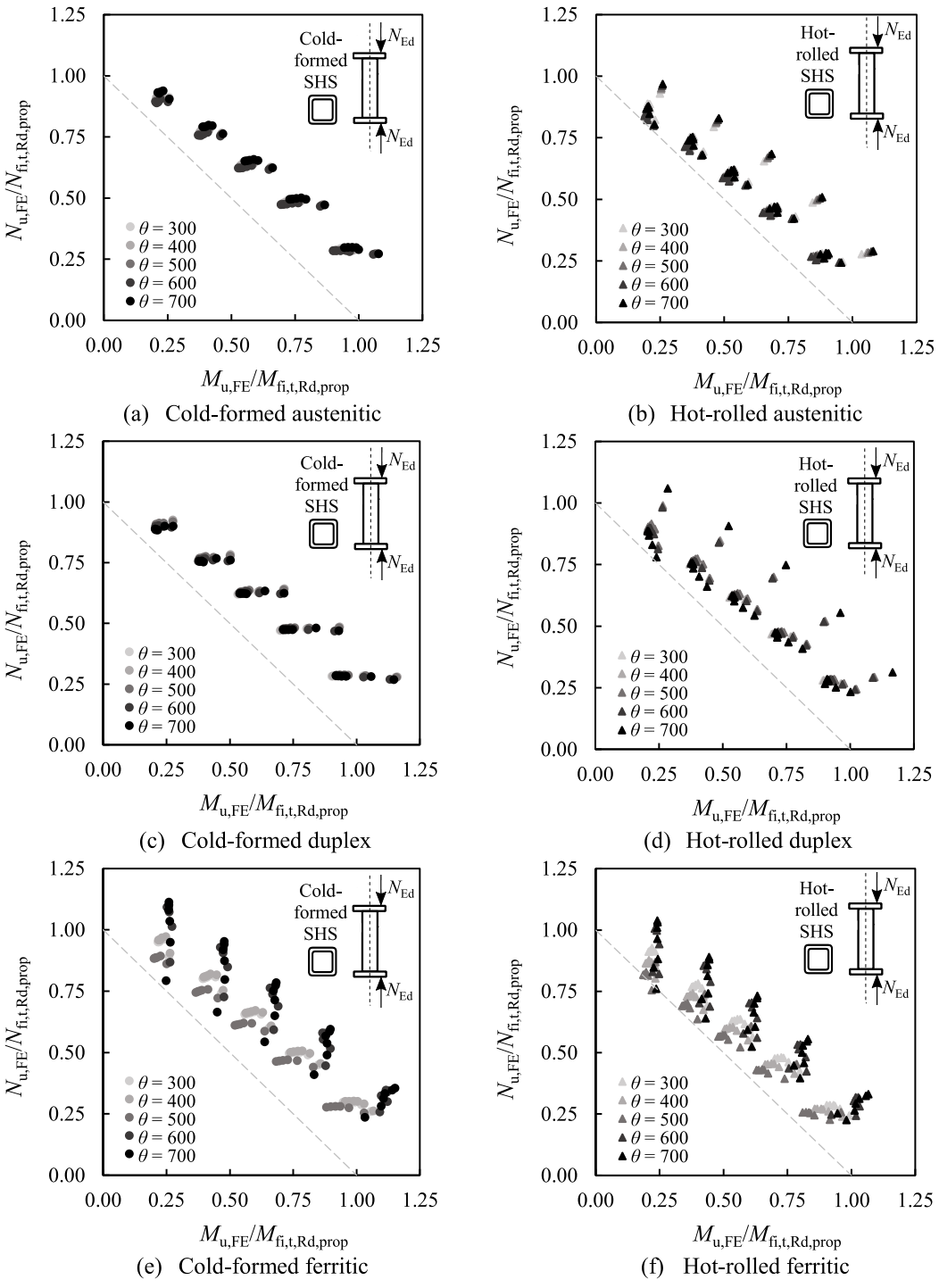

Fig. 21. Interaction relationship between (i) the ultimate compression resistances obtained from FE modelling $N_{u,FE}$ normalised by the cross-sectional compression resistances predicted using the new proposals $N_{fi,t,Rd,prop}$ and (ii) the ultimate bending moment resistances obtained from FE modelling $M_{u,FE}$ normalised by the cross-sectional bending moment resistances predicted using the new proposals $M_{fi,t,Rd,prop}$ for stainless steel SHS under combined compression and bending at elevated temperatures.

steel SHS and RHS subjected to combined axial compression and bending at elevated temperatures. It can be seen from the table that the proposed design rules fulfil all the three fire design reliability criteria of Kruppa [52], while EN 1993-1-2 [3] violates all the three reliability criteria for the most of the considered groups, indicating that the proposed design rules provide significantly more accurate and reliable resistance predictions relative to EN 1993-1-2 [3] for stainless steel SHS and RHS subjected to combined compression and bending at elevated temperatures; the unsafety of the resistance predictions obtained using EN 1993-1-2 [3] can also be observed in Fig. 23.

5.4. Combined bending and shear

In the case of stainless steel SHS and RHS subjected to combined bending and shear at elevated temperatures, this study recommends a design approach similar to that given in EN 1993-1-2 [3]. As described in Section 4.2, when the applied shear force V_{Ed} exceeds half of the plastic cross-section shear resistance $V_{pl} = A_v k_{2,\theta} f_y$(i.e. $V_{Ed} > 0.5 A_v k_{2,\theta} f_y$), the cross-section resistance is reduced by adopting a reduced elevated temperature material strength whereby the adverse effects from high shear forces could be considered. Fig. 24 shows the

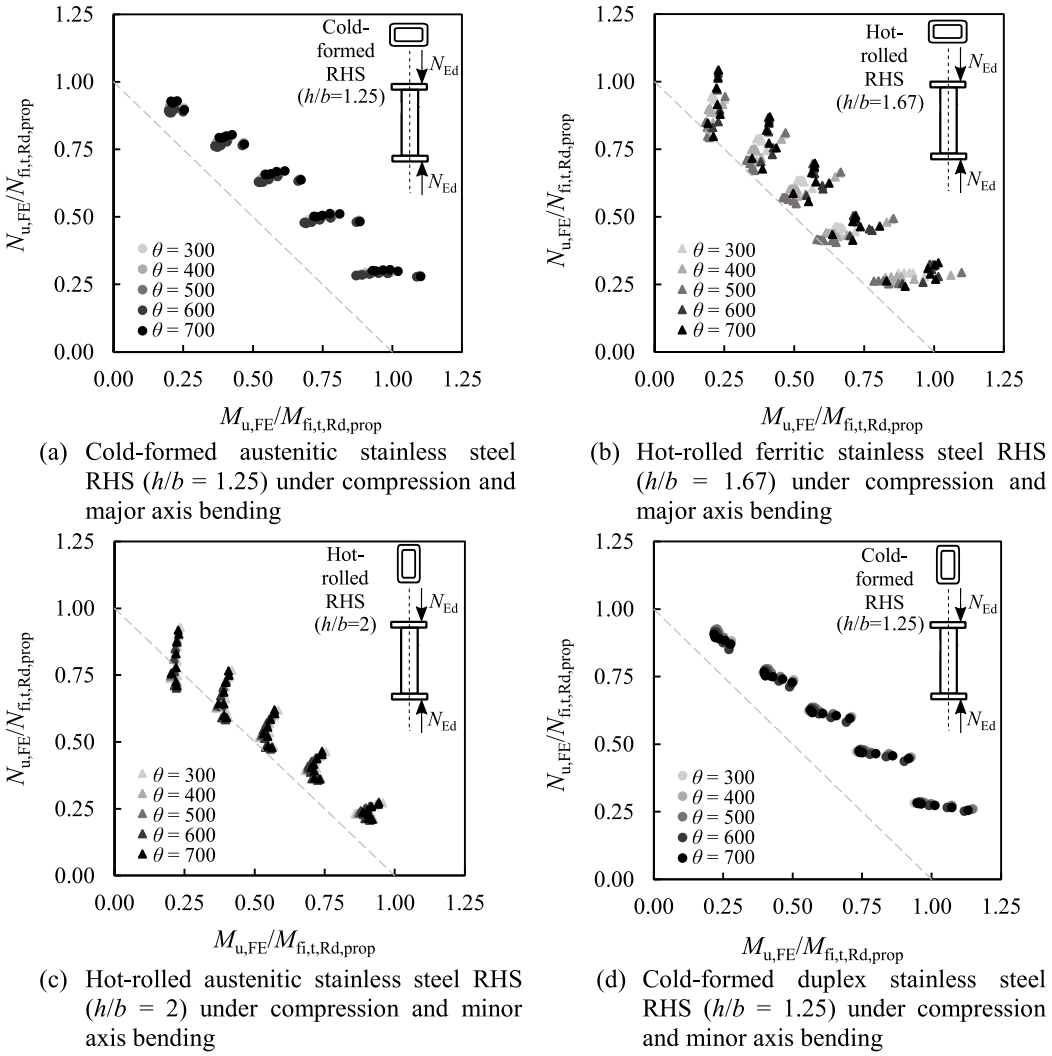

(a) Cold-formed austenitic stainless steel RHS (h/b = 1.25) under compression and major axis bending

(b) Hot-rolled ferritic stainless steel RHS (h/b = 1.67) under compression and major axis bending

(c) Hot-rolled austenitic stainless steel RHS (h/b = 2) under compression and minor axis bending

(d) Cold-formed duplex stainless steel RHS (h/b = 1.25) under compression and minor axis bending

Fig. 22. Interaction relationship between (i) the ultimate compression resistances obtained from FE modelling $N_{u,FE}$ normalised by the cross-sectional compression resistances predicted using the new proposals $N_{fi,t,Rd,prop}$ and (ii) the ultimate bending moment resistances obtained from FE modelling $M_{u,FE}$ normalised by the cross-sectional bending moment resistances predicted using the new proposals $M_{fi,t,Rd,prop}$ for studied examples of stainless steel RHS under combined compression and bending at elevated temperatures.

Table 14
Summary of mean, CoV, maximum and minimum values of the ratios of the resistance predictions obtained from FE modelling $N_{u,FE}$ to those determined using the new proposal $N_{u,prop}$ and the provisions of EN 1993-1-2 [3] $N_{u,EC3}$ for all studied cold-formed and hot-rolled stainless steel SHS and RHS under combined compression and bending at elevated temperatures.

Type	Grade	No.	$N_{u,FE}/N_{u,prop}$				$N_{u,FE}/N_{u,EC3}$			
			Mean	CoV	Max	Min	Mean	CoV	Max	Min
Cold-formed	A	1050	1.20	0.049	1.38	1.02	1.06	0.147	1.46	0.72
	D	1050	1.21	0.061	1.50	1.03	1.10	0.131	1.59	0.80
	F	1050	1.26	0.079	1.51	1.00	1.00	0.144	1.50	0.71
Hot-rolled	A	1225	1.14	0.111	1.76	0.92	0.98	0.164	1.49	0.63
	D	1225	1.18	0.106	1.74	0.91	1.05	0.146	1.48	0.72
	F	1225	1.16	0.085	1.40	0.90	0.96	0.149	1.47	0.63

normalised bending moment–shear interaction diagrams for some of the studied stainless steel SHS and RHS subjected to combined bending and shear at elevated temperatures. Note that in Fig. 24, $V_{u,FE}$ and $M_{u,FE}$ are the ultimate shear and bending moment resistances obtained from the shell FE models, while $M_{fi,t,Rd,prop}$ corresponds to the ultimate bending moment resistance predictions determined through the proposed fire design approach with the reduced elevated temperature material strengths for high shear cases. Note that in some cases where large shear deformations developed and no peak loads were attained in the shell FE models, the ultimate resistances were defined using the applied loads at which the tangent stiffnesses of the load–deformation curves degraded to 1% of the initial stiffnesses, following the approach proposed in dos Santos et al. [58] and also adopted in [59]. As can be seen from Fig. 24, the recommended consideration of bending–shear interaction leads to safe-sided ultimate resistance predictions. Note that due to strain hardening and the effective increase in the elevated temperature material strengths under multi-axial stress conditions, in some cases, cross-sections can continue resisting high shear forces even after the applied bending moments reach the plastic cross-section bending moment resistances, which can be seen from Fig. 24; similar observations were also made in previous studies [60].

In Fig. 25, the ultimate bending moment resistance predictions obtained using the new proposals $M_{u,prop}$ are compared against those from the FE modelling $M_{u,FE}$ for the all studied 3900 cold-formed and hot-rolled stainless steel SHS and RHS members subjected to 3-point bending (i.e combined axial compression and bending) for different cross-section slendernesses. As can be seen from the figure, the proposed approach for the consideration of high shear effects on the ultimate bending moment resistances of stainless steel SHS and RHS at elevated temperatures leads to safe capacity predictions for the considered wide range of SHS and RHS at elevated temperatures.

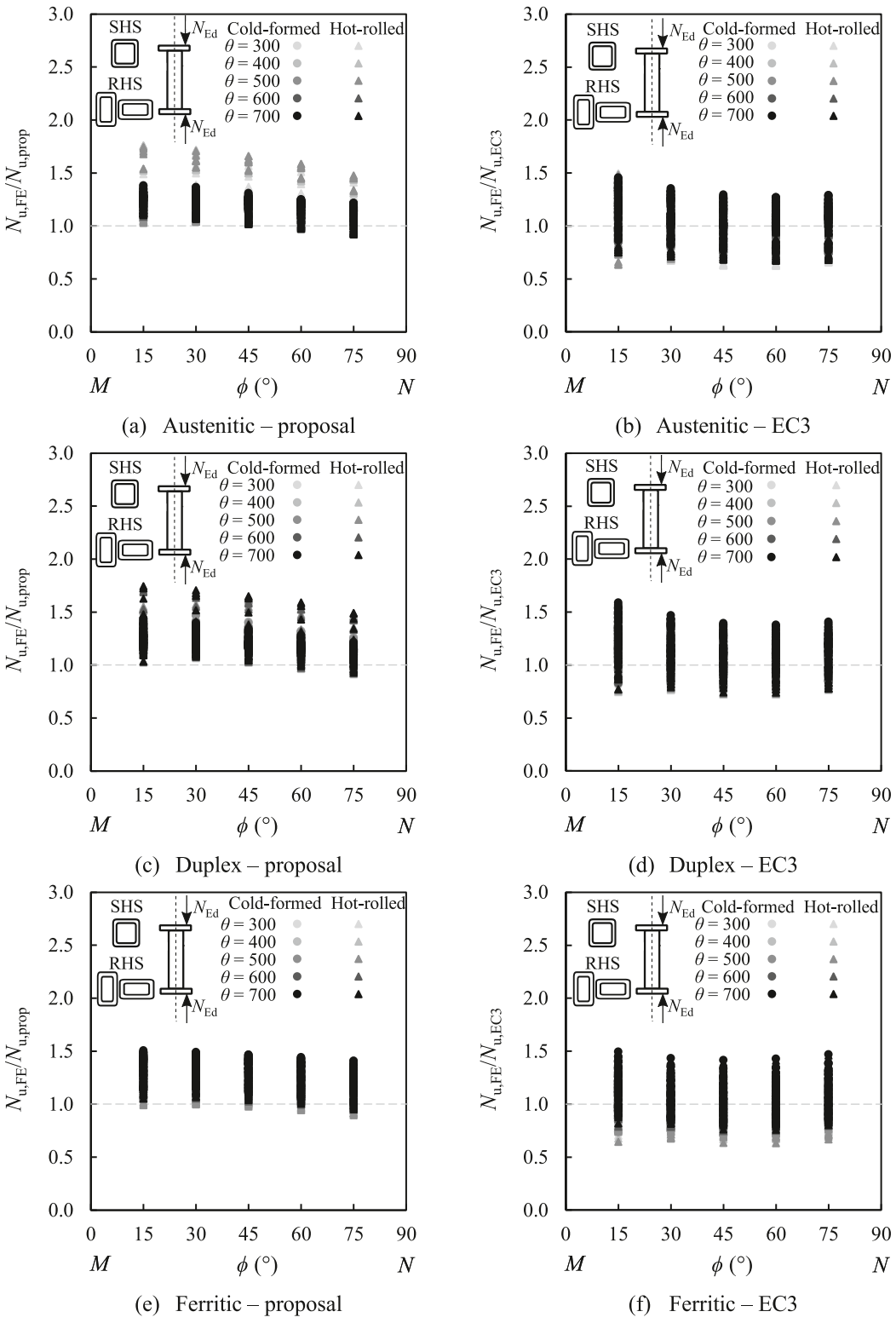

Fig. 23. Assessment of the accuracy of the ultimate axial compression resistances determined through the new proposals $N_{u,prop}$ and the provisions given in EN 1993-1-2 $N_{u,EC3}$ against those obtained from FE modelling $N_{u,FE}$ versus the radial angle ϕ for cold-formed and hot-rolled stainless steel SHS and RHS under combined compression and bending at elevated temperatures.

Note that since this study recommends a design approach in line with that given in EN 1993-1-2 [3] for consideration of high shear effects, the accuracy assessment of only the proposed fire design approach is provided herein. It should also be noted that as shown in Tables 4 and 5, the behaviour of stainless steel SHS/RHS subjected to combined bending and shear at elevated temperatures but not susceptible to shear buckling is taken into account in this study. Future research will focus on a comprehensive investigation of the structural response of stainless

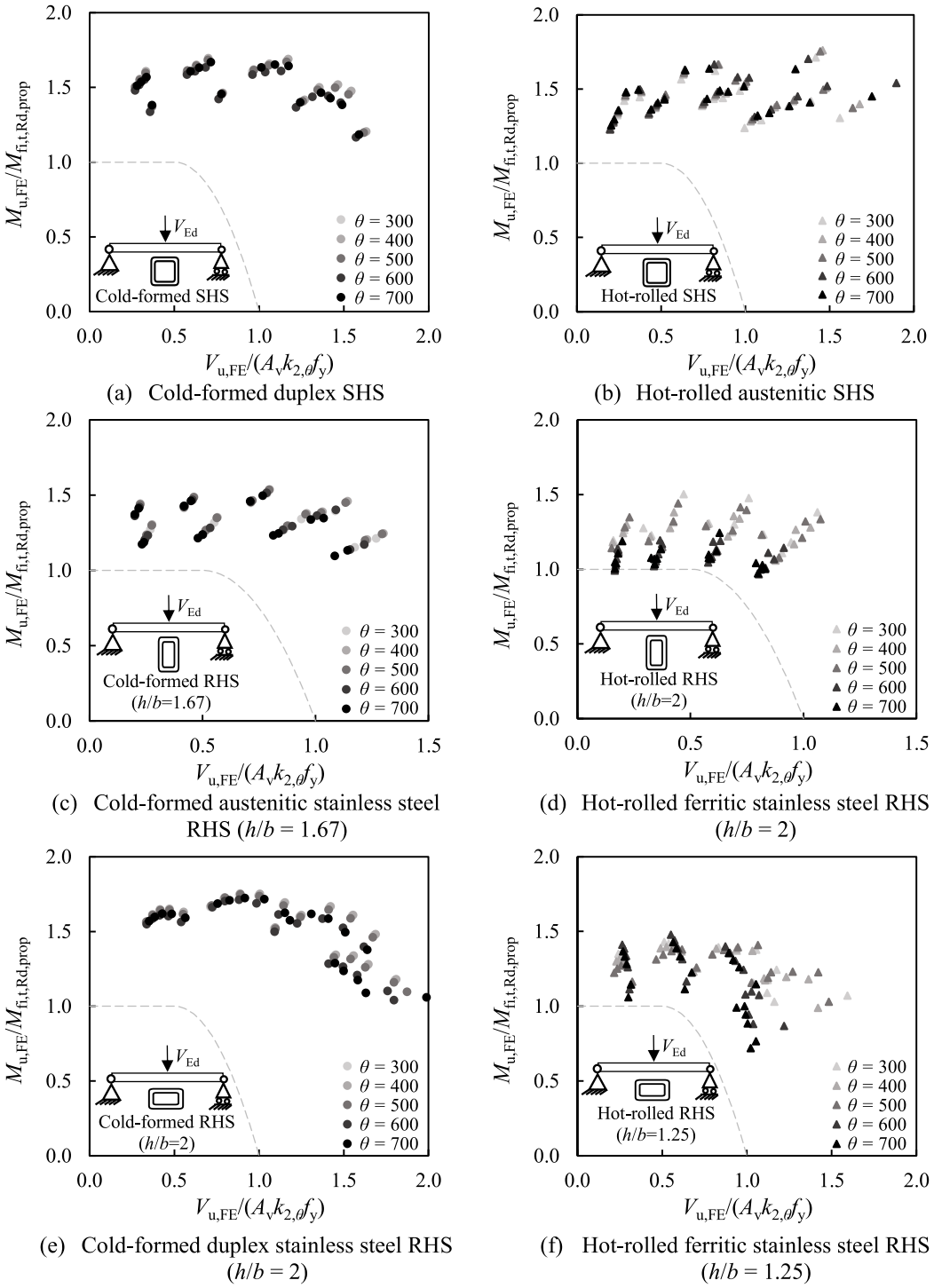

Fig. 24. Interaction relationship between the ultimate shear resistances obtained from FE modelling $V_{u,FE}$ normalised by the cross-sectional plastic shear resistances $A_v k_{2,\theta} f_y$ and the ultimate bending moment resistances obtained from FE modelling $M_{u,FE}$ normalised by the cross-sectional bending moment resistances determined using the proposed design method $M_{fi,t,Rd,prop}$ for studied examples of stainless steel SHS/RHS members under 3-point bending at elevated temperatures.

steel SHS/RHS susceptible to shear buckling at elevated temperatures, with the development of a shear buckling design approach for stainless steel SHS and RHS at elevated temperatures.

6. Conclusions

This study explored the structural response and design of stainless steel square hollow sections and rectangular hollow sections (SHS and RHS) at elevated temperatures. Shell finite element models of stainless steel SHS and RHS members were developed and verified against the results from fire experiments in the literature. After the verification, the developed shell FE models were employed to perform comprehensive numerical parametric studies whereby extensive benchmark structural performance data on the structural response of stainless steel SHS and RHS at elevated temperatures were created. In the numerical parametric studies, both cold-formed and hot-rolled austenitic, duplex and ferritic stainless steel SHS and RHS subjected to different loading conditions (pure compression, pure bending, combined compression

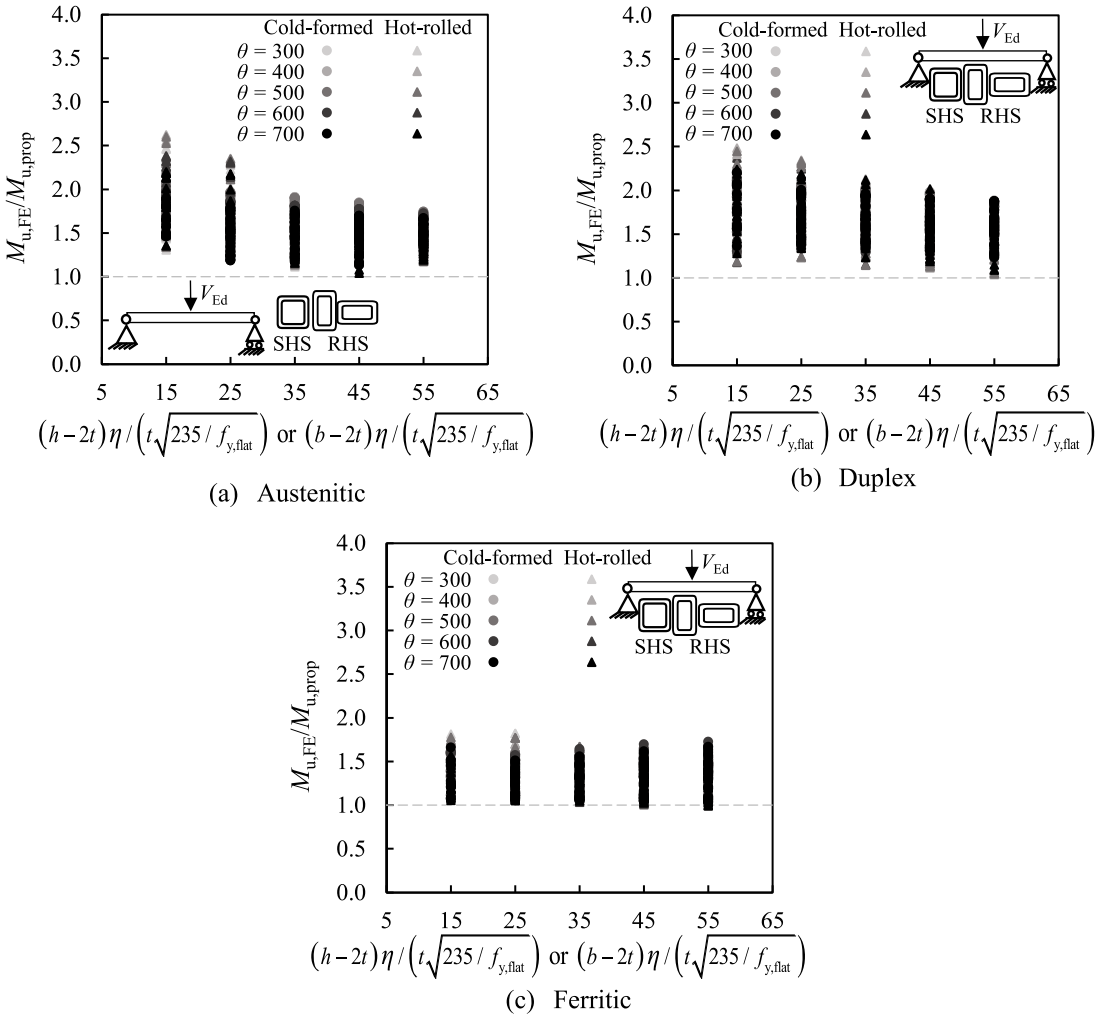

Fig. 25. Assessment of the accuracy of the bending moment resistances determined through the new proposals $M_{u,prop}$ against those obtained from FE modelling $M_{u,FE}$ for cold-formed and hot-rolled stainless steel SHS and RHS under 3-point bending at elevated temperatures.

Table 15
Reliability assessment of the new proposals and the provisions of EN 1993-1-2 [3] for all studied cold-formed and hot-rolled stainless steel SHS and RHS under combined compression and bending.

Type	Grade	Proposal			EN 1993-1-2		
		Criterion 1 (%)	Criterion 2 (%)	Criterion 3 (%)	Criterion 1 (%)	Criterion 2 (%)	Criterion 3 (%)
Cold-formed	A	0.00	0.00	−16.67	14.19*	34.19*	−3.75
	D	0.00	0.00	−17.29	3.05*	28.38*	−7.69
	F	0.00	0.00	−19.87	21.43*	55.62*	2.32*
Hot-rolled	A	0.00	3.67	−11.32	22.29*	54.45*	4.77*
	D	0.00	2.29	−14.50	14.45*	38.53*	−2.62
	F	0.00	4.24	−12.92	27.10*	62.78*	5.91*

*Violated criterion.

and bending and combined bending and shear) with various cross-section geometries and slendernesses ($\bar{\lambda}_{p,H,c}$ = 0.2 – 2) at different elevated temperature levels (θ = 300 °C – 700 °C) were taken into consideration. Shear buckling was not considered in this paper. Thus, the proposed elevated temperature cross-section design rules are limited to the cross-section failure phenomena and parameters taken into account in this study. In total, 13860 stainless steel SHS and RHS members were analysed in the numerical parametric studies, comprising (i) 1140 stainless steel SHS and RHS stub columns subjected to pure axial compression, (ii) 1995 stainless steel SHS and RHS subjected to pure bending, (iii) 6825 stainless steel SHS and RHS stub beam–columns subjected to combined compression and bending and (iv) 3900 SHS and RHS members subjected to 3-point bending (combined bending and shear) at elevated temperatures. The cross-section design rules of stainless steel SHS and RHS subjected to different loading conditions at elevated temperatures were proposed, considering the plate fire design recommendations in [9]. Compared against the benchmark results obtained from shell FE modelling, the accuracy of the new proposals is verified for all the considered cases; the accuracy of the new fire cross-section design proposals is also compared against that of the design provisions of the European structural steel fire design standard EN 1993-1-2 [3]. It was observed that the new cross-section fire design proposals generally provide significantly more accurate and safe-sided ultimate cross-section resistance predictions relative to the design provisions of EN 1993-1-2 [3]. The reliability of the new cross-section fire design proposals and EN 1993-1-2 [3] was also assessed

through the three reliability criteria proposed in Kruppa [52] for the reliability assessment of fire design methods for steel structures. For all the considered cases, it was demonstrated that the new proposals fulfil all the three reliability criteria of Kruppa [52] with the exception of some hot-rolled SHS and RHS subjected to pure compression where some of the reliability criteria of [52] were slightly violated which was primarily due to the adopted conservative local imperfection magnitudes in the FE modelling of this study. For the cold-formed stainless steel SHS and RHS, which are considerably more widely used relative to hot-rolled stainless steel SHS and RHS in practice, and hot-rolled stainless steel SHS and RHS subjected to pure bending and combined axial compression and bending, the new cross-section fire design proposals satisfied all the three reliability criteria of [52]. On the other hand, the provisions of EN 1993-1-2 [3] violated the reliability criteria for a large number considered cases for both cold-formed and hot-rolled stainless steel SHS and RHS at elevated temperatures, indicating that the new proposals provide more reliable resistance predictions relative to EN 1993-1-2 [3] for stainless steel SHS and RHS at elevated temperatures.

CRediT authorship contribution statement

Chunyan Quan: Writing – review & editing, Writing – original draft, Visualization, Validation, Software, Methodology, Investigation, Formal analysis, Data curation. **Merih Kucukler:** Writing – review & editing, Writing – original draft, Supervision, Project administration, Methodology, Investigation, Funding acquisition, Conceptualization.

Declaration of competing interest

The authors declare that there is no conflict of interest.

Data availability

Data will be made available on request

Acknowledgements

The research presented in this paper is funded by the Engineering and Physical Sciences Research Council (EPSRC) of the UK under the grant number EP/034405/01. The authors gratefully acknowledge the financial support of the EPSRC for the research presented in this paper.

References

[1] F. Arrais, N. Lopes, P.V. Real, Numerical study of fire resistance of stainless steel circular hollow section columns, J. Fire Sci. 38 (2020) 156–172.
[2] L. Gardner, Stainless steel structures in fire, Proc. Inst. Civ. Eng. Struct. Build. 160 (2007) 129–138.
[3] EN 1993-1-2, Eurocode 3: Design of Steel Structures-Part 1-2: General Rules – Structural Fire Design, European Committee for Standardization (CEN), Brussels, 2005.
[4] S. Fan, M. Liu, W. Sun, Y. Guo, Y.L. Han, Experimental investigation of eccentrically compressed stainless steel columns with constraints in fire, Fire Saf. J. 99 (2018) 49–62.
[5] EN 1993-1-4:2006 + A1: 2015, Eurocode 3: Design of steel structures – Part 1-4: General rules – Supplementary rules for stainless steels, European Committee for Standardization (CEN), Brussels, 2015.
[6] A. Ranby, Structural fire design of thin walled steel sections, J. Construct. Steel Res. 1 (46) (1998) 303–304.
[7] M. Kucukler, Local stability of normal and high strength steel plates at elevated temperatures, Eng. Struct. 243 (2021) 112528.
[8] C. Couto, P. Vila Real, N. Lopes, B. Zhao, Resistance of steel cross-sections with local buckling at elevated temperatures, J. Construct. Steel Res. 109 (2015) 101–114.
[9] Z. Xing, M. Kucukler, L. Gardner, Local buckling of stainless steel plates in fire, Thin-Walled Struct. 148 (2020) 106570.
[10] prEN 1993-1-2, Final Draft of Eurocode 3: Design of Steel Structures – Part 1-2: General Rules – Structural Fire Design, European Committee for Standardization (CEN), Brussels, 2021.
[11] Z. Xing, M. Kucukler, L. Gardner, Local buckling of stainless steel I-sections in fire: Finite element modelling and design, Thin-Walled Struct. 161 (2021) 107486.
[12] A. Mohammed, S. Afshan, Numerical modelling and fire design of stainless steel hollow section columns, Thin-Walled Struct. 144 (2019) 106243.
[13] Y. Huang, J. Chen, Y. He, B. Young, Design of cold-formed stainless steel RHS and SHS beam–columns at elevated temperatures, Thin-Walled Struct. 165 (2021).
[14] L. Gardner, R.B. Cruise, Modeling of residual stresses in structural stainless steel sections, J. Struct. Eng. ASCE 135 (2009) 42–53.
[15] C. Quan, M. Kucukler, Cross-section resistance and design of stainless steel CHS and EHS at elevated temperatures, Eng. Struct. 285 (2023) 115996.
[16] ABAQUS, ABAQUS/Standard User's Manual. Version 6.17, Dassault Systemes Simulia Corp, USA, 2017.
[17] Y. Cai, F. Zhou, L. Wang, B. Young, Design of lean duplex stainless steel tubular sections subjected to concentrated end bearing loads at elevated temperatures, Thin-Walled Struct. 160 (2021) 107298.
[18] H. Yang, F. Liu, L. Gardner, Performance of concrete-filled RHS columns exposed to fire on 3 sides, Eng. Struct. 56 (2013) 1986–2004.
[19] X. Meng, L. Gardner, A.J. Sadowski, J.M. Rotter, Elasto-plastic behaviour and design of semi-compact circular hollow sections, Thin-Walled Struct. 148 (2020) 106486.
[20] L. Gardner, N. Saari, F. Wang, Comparative experimental study of hot-rolled and cold-formed rectangular hollow sections, Thin-Walled Struct. 48 (2010) 495–507.
[21] EN 10219-2, Cold Formed Welded Structural Hollow Sections Part 2: Tolerances, Dimensions and Sectional Properties, European Committee for Standardization (CEN), Brussels, 2019.
[22] EN 10210-2, Hot-Finished Structural Hollow Sections Part 2: Tolerances, Dimensions and Sectional Properties, European Committee for Standardization (CEN), Brussels, 2019.
[23] H. Fang, T.M. Chan, Resistance of axially loaded hot-finished S460 and S690 steel square hollow stub columns at elevated temperatures, Structures 17 (2019) 66–73.
[24] M. Anwar-us saadat, M. Ashraf, S. Ahmed, Thin-Walled Structures Behaviour and design of stainless steel slender cross-sections subjected to combined loading, Thin Walled Struct. 104 (2016) 225–237.
[25] I. Arrayago, E. Real, L. Gardner, Description of stress–strain curves for stainless steel alloys, Mater. Des. 87 (2015) 540–552.
[26] E. Mirambell, E. Real, On the calculation of deflections in structural stainless steel beams: An experimental and numerical investigation, J. Construct. Steel Res. 54 (2000) 109–133.
[27] K.J.R. Rasmussen, Full-range stress–strain curves for stainless steel alloys, J. Construct. Steel Res. 59 (2003) 47–61.
[28] J. Chen, B. Young, Stress–strain curves for stainless steel at elevated temperatures, Eng. Struct. 28 (2) (2006) 229–239.
[29] T. Manninen, J. Säynäjäkanas, Mechanical properties of ferritic stainless steel at elevated temperature, in: Proceedings of the Fourth International Experts Seminar on Stainless Steel in Structures, 2012, The Steel Construction Institute, Ascot, UK, 2012.
[30] Design Manual for Structural Stainless Steel, fourth ed., Steel Construction Institute (SCI), 2017.
[31] T. Ala-Outinen, T. Oksanen, Stainless Steel Compression Members Exposed to Fire, Research Notes 1864, Technical Research Centre of Finland (VTT), Finland, 1997.
[32] L. Gardner, A. Insausti, K.T. Ng, M. Ashraf, Elevated temperature material properties of stainless steel alloys, J. Construct. Steel Res. 66 (5) (2010) 634–647.
[33] L. Gardner, Y. Bu, P. Francis, N.R. Baddoo, K.A. Cashell, F. McCann, Elevated temperature material properties of stainless steel reinforcing bar, Constr. Build. Mater. 114 (2016) 977–997.
[34] S. Afshan, O. Zhao, L. Gardner, Standardised material properties for numerical parametric studies of stainless steel structures and buckling curves for tubular columns, J. Construct. Steel Res. 152 (2019) 2–11.
[35] L. Gardner, D.A. Nethercot, Numerical modeling of stainless steel structural components-A consistent approach, J. Struct. Eng. ASCE 130 (10) (2004) 1586–1601.
[36] T. Ala-Outinen, Fire Resistance of Austenitic Stainless Steels Polarit 725 (EN 1.4301) and Polarit 761 (EN 1.4571), VTT Research Notes 1760, Espoo (Finland), 1996.
[37] F. McCann, L. Gardner, S. Kirk, Elevated temperature material properties of cold-formed steel hollow sections, Thin-Walled Struct. 90 (2015) 84–94.
[38] EN 1993-1-5, Eurocode 3: Design of Steel Structures Part 1-5: Plated Structural Elements, European Committee for Standardization (CEN), Brussels, 2006.
[39] A.D. Martins, R. Gonçalves, D. Camotim, Numerical simulation and design of stainless steel columns under fire conditions, Eng. Struct. 229 (2021).
[40] M. Jandera, L. Gardner, J. Machacek, Residual Stresses in Cold-Rolled Stainless Steel Hollow Sections, Vol. 64, 2008, pp. 1255–1263.
[41] B. Uppfeldt, T. Ala Outinen, M. Veljkovic, A design model for stainless steel box columns in fire, J. Construct. Steel Res. 64 (2008) 1294–1301.
[42] L. Gardner, N.R. Baddoo, Fire testing and design of stainless steel structures, J. Construct. Steel Res. 62 (2006) 532–543.

[43] J. Pauli, D. Somaini, M. Knobloch, M. Fontana, Experiments on Steel Columns Under Fire Conditions, Vol. 340, ETH Zurich Institute of Structural Engineering IBK Test Report No, 2012.
[44] EN 1363-1, Fire Resistant Tests: Part 1 — General Requirements, European Committee for Standardization (CEN), 2012.
[45] M. Kucukler, Z. Xing, L. Gardner, Behaviour and design of stainless steel I-section columns in fire, J. Construct. Steel Res. 165 (2020) 105890.
[46] B. Young, G.J. Hancock, Tests of channels subjected to combined bending and web crippling, J. Struct. Eng. ASCE 128 (2002) 300–308.
[47] R.D. Ziemian, Guide to Stability Design Criteria for Metal Structures, sixth ed., John Wiley & Sons, 2010.
[48] UK NA to EN 1993-1-4, UK National Annex to Eurocode 3. Design of Steel Structures: Part 1–4: General Rules—Supplementary Rules for Stainless Steels, BSI, 2015.
[49] EN 1993-1-1:2005 + A1: 2014, Eurocode 3: Design of Steel Structures - Part 1-1: General Rules and Rules for Buildings, European Committee for Standardization (CEN), Brussels, 2014.
[50] L. Gardner, A. Fieber, L. Macorini, Formulae for calculating elastic local buckling stresses of full structural cross-sections, Structures 17 (2019) 2–20.
[51] L. Gardner, The continuous strength method, Proc. Inst. Civ. Eng.-Struct. Build. 161 (3) (2008) 127–133.
[52] J. Kruppa, Eurocodes–Fire parts: Proposal for a methodology to check the accuracy of assessment methods, CEN TC 250, Horizontal Group Fire, Document, 1999, pp. 99–130.
[53] N. Lopes, M. Manuel, A.R. Sousa, P. Vila Real, Parametric study on austenitic stainless steel beam–columns with hollow sections under fire, J. Construct. Steel Res. 152 (2019) 274–283.
[54] M. Kucukler, In-plane structural response and design of steel I-section beam–columns at elevated temperatures, Structures 39 (2022) 1045–1062.
[55] M. Kucukler, Lateral instability of steel beams in fire: Behaviour, numerical modelling and design, J. Construct. Steel Res. 170 (2020) 106095.
[56] T. Von Karman, E. Sechler, L. Donnell, The strength of thin plates in compression, Trans. ASME 54 (1932) 53–57.
[57] G. Winter, Strength of thin steel compression flanges, Trans. ASCE 112 (1947) 527–554.
[58] G.B. dos Santos, L. Gardner, M. Kucukler, A method for the numerical derivation of plastic collapse loads, Thin-Walled Struct. 124 (2018) 258–277.
[59] C. Quan, M. Kucukler, L. Gardner, Out-of-plane stability design of steel beams by second-order inelastic analysis with strain limits, Thin-Walled Struct. 169 (2021) 108352.
[60] S.C. Lee, D.S. Lee, C.H. Yoo, Flexure and shear interaction in steel I-Girders, J. Struct. Eng. ASCE. 139 (2013) 1882–1894.